Leaf Area Index in Riparian Forests: Estimation with Airborne Lidar vs. Airborne Structure-from-Motion and the Societal Value of Remotely Sensed Ecological Information

Travis Axe

A thesis submitted in partial fulfillment of the requirements of

Master of Science

University of Washington

2018

Committee:

L. Monika Moskal

Craig Thomas

Akira Kato

Programs Authorized to Offer Degree:

School of Environmental and Forest Sciences

University of Washington

Abstract

Leaf Area Index in Riparian Forests: Estimation with Airborne Lidar vs. Airborne Structure-from-Motion and the Societal Value of Remotely Sensed Ecological Information

Travis Axe

Chairs of the Supervisory Committee:

Dr. L. Monika Moskal

School of Environmental and Forest Sciences

Dr. Craig Thomas

The Evans School of Public Policy and Governance

Remote Sensing technology has expanded tremendously over the past few decades and has created value when integrated into environmental concepts and practices. But there is unmet potential for bolstering ecosystem services and creating additional value for society. Impediments such as the cost and complexity of the technology, and the difficulty of readily assimilating it into a decision-making process, must be overcome to facilitate broader use.

This study demonstrates the capacity for an emerging and inexpensive remote sensing technology to estimate an important ecological indicator and then discusses the broader implications for societal value. First, we compare the estimation of effective leaf area index (LAI_E) of heterogeneous riparian forests between two remote sensing methodologies: discrete-return Airborne Laser Scanning (ALS) and airborne structure-from-motion (SfM). LAI_E is an

indispensable component of process-based ecological research and can be associated with a variety of ecosystem services. SfM data acquisition is more frequent and inexpensive compared to ALS, but its capabilities less explored. Two point-cloud data files for each technology were evaluated using respective field-measured reference data. SfM shows promise: a combinational linear regression revealed that the distribution elevation values of upper-canopy point returns and the elevation values representing mid and max stand-level, when paired grey-level co-occurrence matrix (GLCM), can estimate LAI_E ($r^2 = 0.62$). Although it did not perform as well as ALS, which has more data representing light attenuation behavior ($r^2 = 0.66$), SfM as an alternative methodology for remotely sensing ecological data has demonstrated potential and warrants further investigation.

Next, we discuss how remotely sensed ecological information like LAI_E can create value for society. We provide a primer on the ways in which society values the environment and how these values may be perceived and quantified, and the dynamic behavior that exists between them. We then introduce a major policy tool used in quantifying these values, benefit cost analysis, and why it is useful for framing environmental issues and how remote sensing can contribute to its outcomes. Finally, we review remote sensing applications used in increasing our understanding of society's interaction with the environment and existing opportunities for value addition.

Table of Contents

List of Terms

- **ALS**: airborne laser scanning
- **BCA**: benefit cost analysis
- **Canopy**: a polygon surrounding the outer edges of the foliage, without subtracting any normal spaces occurring between the leaves of plants. Overlapping crowns within a species or growth habit are not double counted; the maximum possible cover is 100%
- **Canopy cover** is defined as the area of ground surface covered by a vertical projection of the canopy of a vascular plant.
- **CWD:** coarse woody debris
- **DBH:** diameter at breast height; the point at which a tree's stem diameter is measured
- **DHP**: digital hemispherical photography

- **DHP_LAI$_E$**: effective leaf area index derived from digital hemispherical photography, used as reference data

- **DSM:** digital surface model

- **Dynamic Efficiency:** incorporating the difference in value of benefits and costs as they vary over time

- **Ecosystem**: a biological community of interacting organisms and their physical environment. When considered in conjunction with mankind's influence and economic markets, it is referred to as a resource environment.

- **Elev.p95:** the 95th percentile point elevation with respect to the entire point cloud

- **EVI:** enhanced vegetation index is an optimized vegetation index designed to enhance the vegetation signal with improved sensitivity in high biomass regions and improved vegetation monitoring through a de-coupling of the canopy background signal and a reduction in atmosphere influences.

- **Forest structure:** the spatial arrangement of the components of a forest ecosystem, and describes properties such as the horizontal and vertical distribution and abundance of vegetative elements

- **fPAR:** a parameter that signifies the portion of plants using active photosynthesis

- **Gap fraction:** the probability of sun light rays not penetrating into the understory of a tree canopy

- **Image texture:** the quantification of the spatial variation of image tone values that are related to changes in the spatial distribution of forest vegetation, both in the vertical and horizontal dimension.

- **IRR:** Internal Rate of Return signifies the point in which the Net Present Value of a policy option equals zero.

- **LAI**: leaf area index the total leaf surface area per unit ground area

- **LAI$_E$**: effective leaf area index, which is LAI plus associated vegetation matter like branches and stems

- **FIA**: the forest inventory and analysis program of the U.S. forest service provides the information needed to assess America's forests

- **Lidar**: light detection and ranging

- **MA:** Millennium Ecosystem Assessment

- **Negative Externality:** a cost that is suffered by a third party as a result of an economic transaction. In a transaction, the producer and consumer are the first and second parties, and third parties include any individual, organization, property owner, or resource that is indirectly affected.

- **NDVI:** normalized difference vegetation index.

- **Opportunity costs**: the value of goods/services that would have been produced had these resources been used instead in the best alternative way

- **Point cloud:** unless the words "Lidar" or "SfM" are explicitly used, point cloud is used to refer to the general technology of both platforms

- **Policy:** a relatively stable, purposive course of action followed by actors or institutions in dealing with a problem or issue

- **PPF**: production possibility frontier is a curve depicting all maximum output possibilities for two goods, given a set of inputs consisting of resources and other factors. The PPF assumes that all inputs are used efficiently.

- **Primary markets** include all stakeholders, assets, and processes that are directly affected by a policy, and may include "missing parts" of the market, or, the externalities. **Secondary markets** include everything that is indirectly affected.

- **Primary production:** the synthesis of organic compounds from atmospheric or aqueous carbon dioxide. It principally occurs through the process of photosynthesis, which uses light as its source of energy, but it also occurs through chemosynthesis, which uses the oxidation or reduction of inorganic chemical compounds as its source of energy. Almost all life on Earth relies directly or indirectly on primary production.

- **PV:** The Present Value, in real dollars, of a benefit or cost within a proposed benefit cost analysis

- **R_c:** the total number of canopy returns from a respective plot point cloud

- **$\%r_{c1}$:** the percentage of first returns classified as canopy returns from a respective point cloud

- **R_g:** the total number of ground returns from a respective plot point cloud

- **R_t:** the total number of returns from a respective point cloud. ($r_c + r_g$)

- **Remote Sensing:** the technology, science and art of obtaining information about an object, area, or phenomenon through the analysis of data acquired by a device that is not in contact with the object, area, or phenomenon under investigation.

- **Resource environment:** the flow of all environmental resources and functions that directly and indirectly benefit mankind.
- **SfM:** structure from motion is a photogrammetric range imaging technique for estimating three-dimensional structures from two-dimensional image sequences that may be coupled with local motion signals. It is studied in the fields of computer vision and visual perception
- **Tree height** is defined as the vertical distance between two horizontal planes: one plane passing through the highest twig and the other through the base of the tree at mid-slope. Tree height is not synonymous with trunk
- **WA-DNR**: Washington State Department of Natural Resources

List of Figures

List of Tables

Background

Leaf Area Index (LAI) is broadly defined as the total leaf surface area per unit ground area (Asner et al., 2003). Because it quantifies vegetation, it is related to many processes such as photosynthesis, evaporation, transpiration, rainfall interception, biosphere-atmosphere interactions, gross primary production, insect damage, carbon flux, and overall forest-health monitoring (Gheng and Moskal, 2009). LAI can be used to help assess forest health, resilience, and change over time (Waring 1985). It is a dimensionless variable that serves as an important biophysical parameter for a variety of ecological functions, and therefore contributes to our understanding of how and why natural resources change over time. Some researchers claim that LAI is the single most important variable derived from remote platforms for quantifying energy and mass exchange by plant canopies (Running 1988).

Remote sensing can improve the integrity of an environmental policy by supplementing the knowledgebase of ecosystem processes and their respective social counterparts. By measuring environmental indicators like LAI across large landscapes, remote sensing can provide additional data and supplement methods used in valuating environmental resources and processes. By offering precise, spatially continuous, and frequent observations, remote sensing yields information that enhances our understanding of ecological quantities, processes, and the subsequent interactions with social systems.

The aims of the study were to:

(1) Obtain LAI_E estimates from highly diverse and heterogeneous riparian forests using two distinct remote sensing platforms as input data
(2) Evaluate and compare how two models perform with each type of remotely sensed input: a combinational linear regression and a Beer-Lambert law based approach
(3) Discuss the societal value of the operation application of the scientific information provided by this kind of remote sensing technology.

The first two objectives are located in Chapter 1, the last objective in Chapter 2. A brief synopsis of each chapter is included below.

Chapter 1

The study examined riparian forest-buffers in the Mashel River watershed in Washington State, which was chosen for both its hydrologically complex landscape and its range of forest types. LAI_E reference data were first compared to the output of ALS analysis, which replicated several models used in similar studies. These results showed that the penetration rate of lidar first returns was strongly related to LAI_E even when keeping the elevation threshold of penetration consistent with the actual height of the field camera. Models that tested light attenuation variations in accordance with the Beer-Lambert law saw similar results. However, these were more limited due to the complexity of leaf angle distribution, canopy structure, and terrain.

The reference data was then compared to Structure-from-Motion (SfM) output, which utilized the point cloud of a digital surface model (DSM), rendered from airborne photography. A combinational linear regression showed promise in estimating LAI_E, by utilizing the distribution elevation values of upper-canopy point returns and the elevation values representing mid and max stand-level totals for each observation's respective point cloud. A spectral analysis yielded a second-order statistics grey-level co-occurrence matrix (GLCM) entropy: adding this variable further improved the regression results. SfM performed less well in the Beer-Lambert approach because of the relative lack of appropriate ground points, even when altering the elevation of the penetration threshold.

Chapter 2

The second chapter is for researchers and practitioners who have limited understanding in how remote sensing science may be applied to environmental policy and create value to society. It is for those who wish to begin establishing the foundational knowledge required for bridging the gap between remote sensing science and social science. This requires, at the least, a general understanding of how environmental issues are translated into and affected by economics. This chapter provides a discussion that one can utilize to better understand the societal value of the operation and policy application of the scientific information provided by remote sensing technology.

Chapter 1: Estimating Effective Leaf Area Index in Heterogeneous Riparian Forests:

Airborne Lidar vs. Airborne Structure-from-Motion

Travis Axe, 2018

1.1 Introduction

Measuring Leaf Area Index (LAI) is accomplished through two broad methods: "direct" methods which involve destructive sampling and litter fall collection, and "indirect" methods which involve optical, remote sensing instruments and radiative transfer models. Direct, ground-based measurements and subsequent analyses can be very costly, time-consuming, and are not feasible for frequent data collection over large areas. Indirect remote sensing technologies can overcome these obstacles by offering large spatial coverage in a fraction of the time. There are two primary categories of remote sensing: active and passive. Furthermore, these can be applied to many different platforms: terrestrial, aerial, unmanned aerial vehicle (UAV), and satellite (Zheng and Moskal, 2009).

Two primary factors affect the accuracy of LAI estimation: non-random distribution of tree foliage, and light obstruction from canopy components such as branches, boles, and stems. For example, the non-randomness of shoot position has been shown to reduce indirect measurement of LAI by approximately 35% for a Douglas-fir canopy (Zheng and Moskal, 2009). Most studies (including this one) have derived Effective Leaf Area Index (LAI_E) which does not correct for the non-random distribution of foliage or the presence of non-foliage elements like tree branches. In order to arrive at true LAI, one would need to perform certain corrections, which have been explored in other studies and are outside the scope of this research (Leblanc 2005).

This study compares, contrasts, and explores two distinct remote sensing approaches in estimating LAI_E:

1. **Airborne Laser Scanning (ALS)** is an aerial-active remote-sensing method that utilizes lidar (light detection and ranging) technology. Lidar pulses strike the tops of trees from different angles, mimicking how solar radiation might interact with and permeate through a forest canopy. Laser pulses reflect off varying levels of the canopy, capturing some of its structural information. Some pulses will completely penetrate the upper canopy through gaps and openings, reflecting off various sub-canopy objects. This ratio of data points between canopy and sub-canopy (ground) can be associated with the probability that light will permeate a given canopy. This is the essence of "gap fraction" theory, which, in turn, is mathematically related to LAI (Solberg 2008).

2. **Structure-from-Motion (SfM)** is a passive remote sensing method that uses a set of images and computer processing to create a collective three-dimensional surface (DSM). This approach utilizes traditional stereoscopic photogrammetry as well defined geometrical features captured in multiple images from different angular viewpoints which are used to generate depth (Snavely et al. 2007). Furthermore, the rendered DSM from software can output a variety of formats, including a point cloud. Although the general structure and point distributions vary greatly from a Lidar-derived point cloud, this format allows a direct comparison between the two remote sensing platforms by inputting standardized data into the same models. In this study we utilize aerial imagery acquired through the USDA's NAIP program (*See 1.2.2 SfM Data Acquisition*).

ALS can characterize forest structure in large spatial and temporal scales. Because of ALS' ability to permeate forest canopy, it has proved effective in quantifying leaf area of dense and mixed forest types. Several ALS-based methods for estimating LAI have been previously studied and demonstrated (Richardson, 2009; Coops, 2007; Solberg, 2006; Morsdorf, 2006; Riano, 2004; Lim, 2003;) and ALS can also be used to estimate other important forest metrics like height, diameter at breast height, crown diameter, stand-density, etc. (Moskal, 2015; Andersen, 2005; Evans, 2009). While ALS has demonstrated great value, it does have several limitations. Lidar acquisitions can be very costly, so continuous mensuration for decision-making support or other types of programs becomes less feasible. Moreover, ALS products are usually acquired through a third-party vendor, and might not necessarily meet the exact needs of the researcher (Westoby et al., 2012). Lidar technology is also very dynamic and evolves continuously, so even if multiple acquisitions are financially possible, it becomes quite difficult to compare datasets overtime (Moskal and Cooke, 2015).

SfM offers some key advantages over ALS, which could make it a more feasible alternative for ongoing assessment of some ecosystem services. First, aerial imagery acquisitions are far less expensive and can be obtained from joint-financed efforts like the NAIP program (Westoby et al., 2012; Archived NAIP Data, 2018). Furthermore, past stereographic aerial imagery could be utilized to obtain historical ecological data and facilitate better long-term change-analysis research. SfM also has the advantage of assessing forest canopy texture from high spatial- and

spectral-resolution imagery. Image texture is a quantification of the spatial variation of image tone values that are related to changes in the spatial distribution of forest vegetation, both in the vertical and horizontal dimensions (Wulder et al., 1996).

SfM has demonstrated success when compared to lidar in a variety of forest-based applications: estimating vineyard leaf area index (Mathews and Jensen, 2013); estimating canopy height models (Dandois and Ellis, 2015) and canopy cover models (Wallace, 2013); change detection of river systems (Fonstad et al, 2013); and high-precision surveying of environmental-support structures in open landscapes (Schwind 2018), with. SfM and ALS can be combined to significantly improve vegetation classification and mensuration when acquisitions are acquired simultaneously (Chianucci et al., 2016). Still, many results are wanting and unique challenges exist. Most recent findings revealed that SfM is generally not as accurate in estimating ecological indicators as ALS and is sensitive to several factors: the time of year of the acquisition (leaf-on vs. leaf-off), the density of the tree canopy, the appropriate assumption of leaf angle distribution, the flight pattern consistency, the degree of image-overlap, the spatial- and spectral-resolution of the acquisition, and the configuration of computational processing algorithms. Further research is needed to overcome these limitations and continue exploring SfM's capacity to assess ecological phenomena. If accuracy, consistency, and ease-of-use of SfM can be proven comparable to lidar, SfM could be employed as a viable, low-cost alternative for continuous large-scale ecosystem assessment.

This chapter compares SfM to ALS for estimating LAI_E across a complex watershed in the Western Cascade Range of Washington State. Evaluated forest-plots are all located within riparian buffers that represent an array of tree species, forest-management types, and geographic terrain. Because the focus is on comparing the two platforms, and not an exploration of LAI-estimation methodologies, a literature review was used to narrow the selection of what methodological approach to use for estimating LAI_E. Based on the best results reflecting similar forest compositions as our study site, a Beer-Lambert law based model was chosen. This is founded on physical law which quantifies light attenuation through a surface (*See 1.2.3 Beer-Lambert Law*). This approach is much less sensitive to differences in tree species like other LAI-modeling techniques (Vose et al. 1995); remains consistent throughout changes in spatial scale and heterogeneous forests; and proved more successful than comparable models in similar forest

types and regions of the Pacific Northwest (Richardson 2011). In the Beer-Lambert law approach, LAI_E is associated with the probability of radiation permeating a canopy. But an increasing proliferation of leaves, needles, stems, and branches creates conditions that are difficult for aerial lidar pulses to penetrate, and even more difficult for photography to capture. Other studies comparing the ability of ALS and SfM to assess canopy conditions also conclude that the visual occlusion caused by upper forest canopies limit the ability of SfM to fully account for all canopy closure and leaf area (Wallace et al. 2016). This encouraged us to pursue a secondary alternative for estimating LAI_E.

The second model utilized a combinational linear regression technique (*See 1.2.3 Combinational Linear Regression)*. This allowed us to explore other features of a SfM point cloud that are not as dependent on canopy light permutation. A set of over 100 explanatory variables derived from point cloud software were compared and tested in thousands of combinations in order to find an optimal linear regression fitted for LAI_E. The explanatory variables capture characteristics related to elevation, intensity, classification (ground vs. canopy), and other statistically-derived values. This same approach for estimating LAI_E has also been tested using UAV imagery (Mathews 2013).

We utilized 113 forestry stands as reference data. These were measured by a field crew from June-September, 2016 in the Mashel River watershed in Washington State. A hemispherical camera was used for measuring crown closure from the ground while other traditional forest mensuration captured individual tree species, DBH, height, crown height, and crown diameter, along with other ancillary information. Processing digital hemispherical photography through specialized software rendered LAI_E by discriminating between sky and non-sky pixels within the image. This reference data was used for accuracy assessment and is referred to as DHP-LAI_E.

The aims of the chapter were to:

(1) Obtain LAI_E estimates from highly diverse and heterogeneous riparian forests using two distinct remote sensing methodologies: ALS and SfM
(2) Evaluate and compare performance by testing input data against two LAI_E estimators:
    a. A combinational linear regression
    b. A Beer-Lambert law model.

1.2 Materials and Methods

The first sections of this chapter will establish the study site, describe the acquisition and pre-processing for ALS and SfM, elaborate on the two primary models used for estimating LAI_E, and describe the methods used for accuracy assessment.

1.2.1 Study Site

The fieldwork was conducted in the Mashel River watershed in southeastern Pierce County, Washington State. The Mashel is over 57,000 acres with 530 miles of streams and a variety of tree species. Forest stands at lower elevations of the study site have balanced mixtures of conifer and deciduous trees, while stands in the eastern, higher-elevation areas are more conifer-dominant. Three-quarters of all trees surveyed during field collection are composed of three dominant species: Douglas fir (*Pseudotsuga menziesii*), western hemlock (*Tsuga heterophylla*), and red alder (*Alnus rubra*). Land-ownership in the Mashel watershed is divided between public, tribal, private-personal, and private-timber entities. Thus, the forests in the watershed capture a range of management and age structures, which allow a complex landscape to be applied in the remote-sensing-based modeling.

Field plots were defined as cylinders with a 12.8m (42 ft.) radius: the dimension of height both applicable to ground, forest-mensuration and lidar/SfM point clouds. An initial set of potential plot locations was created based on geospatial considerations and a stratification of ALS-derived forest characteristics: namely, proximity to stream and man-made objects, and forest stand 80^{th} percentile height and canopy cover. A final set was randomly derived from this, and ultimately 113 plots were successfully measured and documented. This included the exact geographic location, forestry metrics, distance-to-stream, and subjective canopy assessment. Photographic captures of canopy-from-ground for each plot were used as the primary reference data for evaluating LAIE accuracy. Reference data are independent sources of information that allow remote sensing specialist to relate patterns in digital space to real quantities or phenomena on the earth's surface (Campbell 1996). Details of accuracy assessment are covered in 1.2.4. For more information pertaining to the study sight or methodology regarding the field collection see Appendix A.

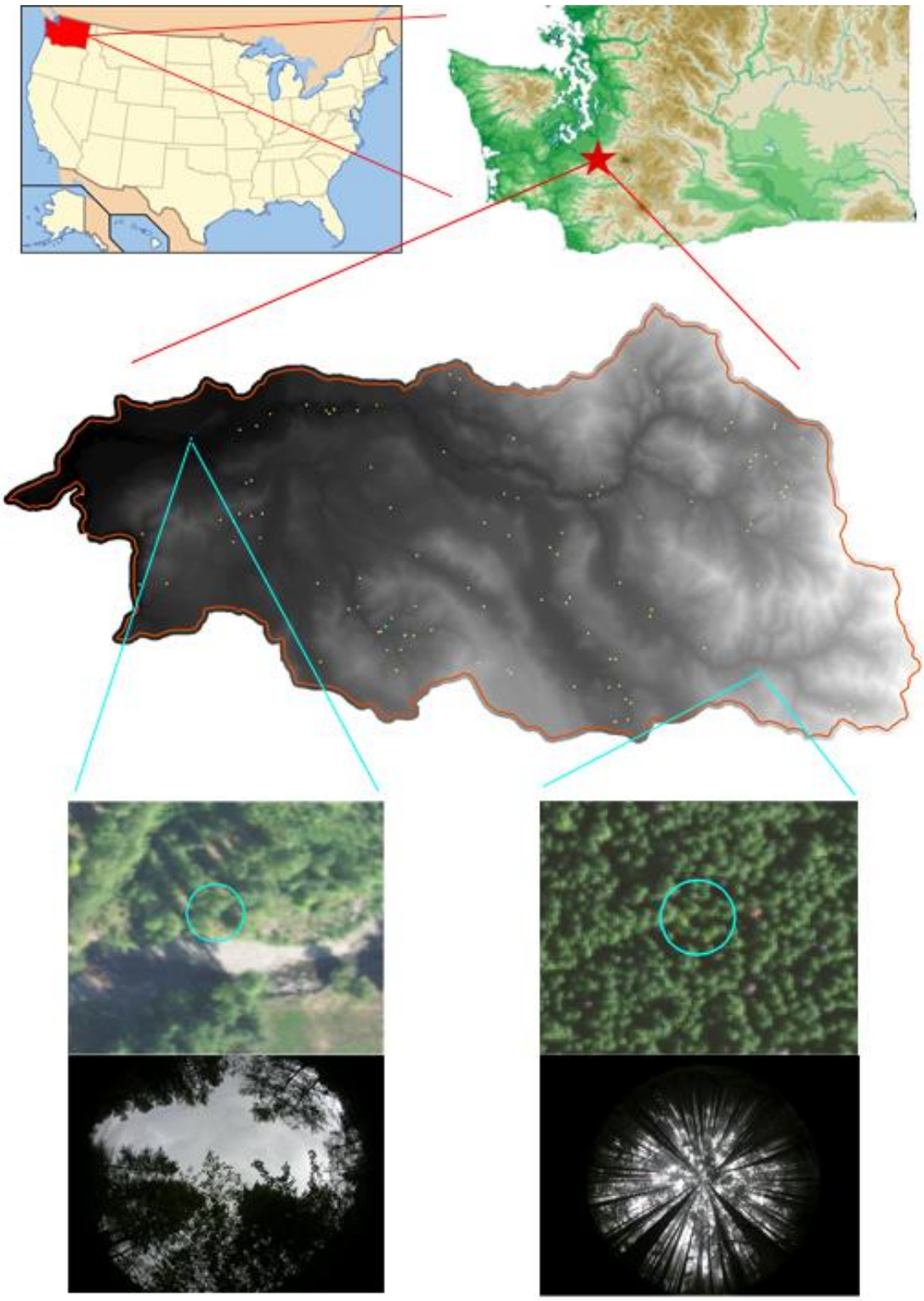

Figure 1. *Project study site. Top images provide context, middle image represents a Digital Elevation Model of the study site with respective field plots, and the bottom images show two examples of field plots from the perspective of both NAIP imagery and Digital Hemispherical Photographs.*

1.2.2 Remotely sensed Data

Aerial Lidar Data Acquisition

The lidar data for this project was collected by Watershed Sciences Inc. (now called Quantum Spatial) for Pierce County in Washington State. The dataset was made publicly available through the Puget Sound LIDAR Consortium (PSLC). Data were acquired between October 2010 and September 2011, processed, and then provided to Pierce County in 21 separate deliveries: spanning a total of 933,000 acres. Watershed Sciences provided processed point data files in LAS 1.2 format, and digital elevation model (DEM) ground surface files in ERDAS Imagine IMG format with three-foot resolution.

Collection date	June 2011
Aircraft	Cessna Caravan 208
Sensor	Leica ALS60
Laser pulse density	> 8 points/m^2
Laser pulse rate	83,000 kHz to 105,900 kHz
Flying height	900 to 1,300 m
Scan angle from nadir	± 30°
Horizontal accuracy	~ 3-5 cm
Vertical accuracy	~ 3-5 cm

Table 1. *Lidar Specifications*

SfM Data Acquisition

The National Agriculture Imagery Program (NAIP) set of imagery used for this project was collected in 2015 by the USDA Farm Services Agency.

Collection date	June 2015
Aircraft	Cessna Caravan 208
Sensor	UltraCam Eagle
Altitude	1,800 m
Image	8-bit GeoTIFF
Sidelap	60%
Spectral bands	Red, Green, Blue, NIR
Resolution	1 m
Horizontal accuracy	< 6m

Table 2. *Airborne imagery specifications*

SOCET GXP is an advanced geospatial intelligence software that utilizes imagery from satellite and aerial sources to identify, analyze, and extract ground features. NAIP imagery was processed with this software to render point data files in LAS 1.2 format (same as ALS). As a part of this system, the Automatic Spatial Modeler (ASM) Module is designed to generate 3-D point clouds. ASM can extract dense 3-D point clouds from NAIP stereo images by performing both local and globalized analysis across a landscape. It processes every individual pixel to maximize accuracy in predicting elevation.

Similar to the lidar data processing, 113 individual SfM point cloud cylinders were clipped to be used and compared with their respective field plot locations. For key processing decisions and more information regarding the specific development of the SfM point cloud, see the developer's strategy file for ASM software in Appendix D.

Point Cloud Processing

Fusion software (McGaughey, 2016) contains multiple features for processing, viewing, and analyzing digital point clouds. Input data from both remote sensing platforms was processed through Fusion's ClipData feature to normalize the vegetation heights above a constant ground elevation. This produced a dataset where the Z value for each point represents the true elevation of that point above ground level. Because these individual point returns can collectively quantify three dimensions, point cloud data can be processed to estimate canopy percent cover, and by association, LAI_E.

Another Fusion feature, CloudMetrics, calculates several different cover metrics, all of which are different ratios of crown to non-crown returns. The theory behind these metrics is that the denser the canopy, the less the laser will penetrate below the canopy, resulting in fewer ground returns. While this is more evident in the results of lidar point cloud analyses, the intuition remains the same for SfM point clouds. Although there are dozens of variables produced in Cloudmetrics output, there are several derived variables which quantify canopy cover. To achieve this, however, Cloudmetrics relies on an explicit "threshold" elevation height in order to calculate canopy cover metrics. It is essentially addressing the question, at what height above ground level must light pass through to be considered "non-canopy" or "ground" data (hereafter, "ground"). This canopy/ground threshold therefore delineates all returns as either "canopy" or "ground".

Figure 2 provides a visual illustration of this concept. The available canopy cover metrics, along with the remaining exhaustive set of CloudMetrics outputs, are available in Appendix C. Because this variable can alter the outcome of model input data significantly, several variations were tested against both input platforms in order to determine which threshold, and corresponding dataset, would be used in final analyses. These pre-processing details can also be found in Appendix C.

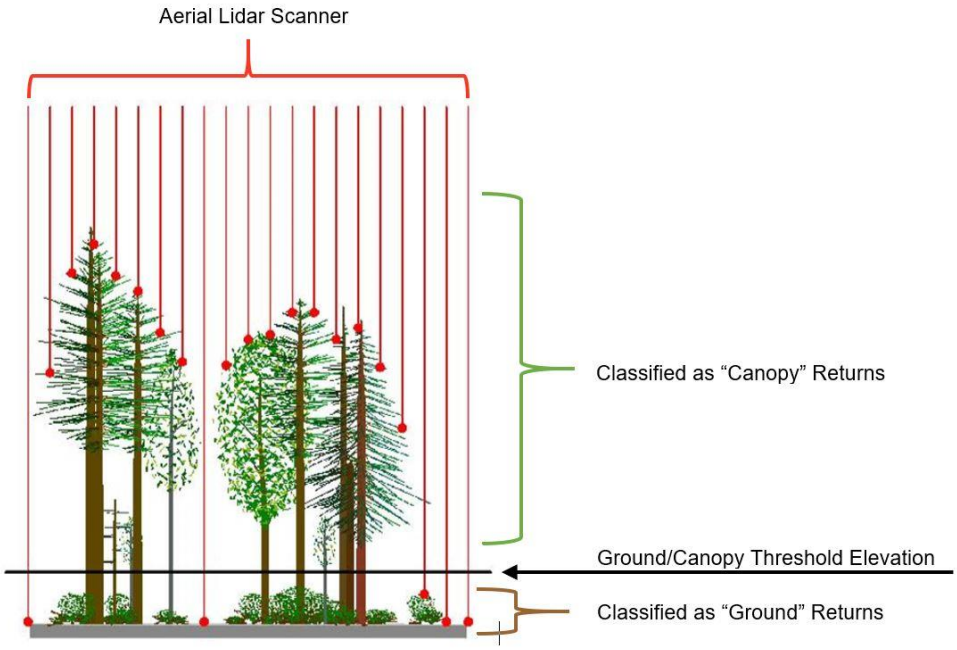

Figure 2. *An illustration conveying the concept of delineating between canopy returns and ground returns using a specified canopy/ground threshold.* Source*: base graphic from FUSION manual (McGaughey, 2016), with modifications by the author (Axe, 2018).*

1.2.3 Modeling LAI_E

Combinational Linear Regression

CloudMetrics outputs over 100 variables for each respective point cloud. Running combinational linear regression helped to confirm previous lidar research and to better understand the structural

implications of a SfM point cloud. So, the entire Cloudmetrics output for each dataset was run through a procedure that tests many combinations of potential explanatory variables, interactions, and transformations in order to find the linear regression best-suited for describing the DHP-LAI_E. The heuristic is as follows:

- Produce best three models using a single explanatory variable.
- Repeat this first step but using two, three, then four explanatory variables.
- Repeat all the above and consider interaction terms.
- Check to see if square-rooting, cube-rooting, or logging reduce any heteroskedacity. If so, repeat all above with the transformed response.
- Deprecate any models that contain non-significant coefficients.
- Perform the Breusch-Pagan, Ramsey's RESET, Rainbow, and Allen's PRESS test for all models. Deprecate any models that are not at least tied for failing the fewest tests.
- Of the final model candidates, select one with the lowest AIC

The Breusch-Pagan test determines if the variance of the errors from a regression is dependent on the values of the independent variables, thus testing for heteroskedasticity in a linear regression model. Ramsey RESET tests if a model suffers from mis-specification. The Rainbow test checks that the regression is correctly modelled as linear and the PRESS statistic is calculated as the sums of squares of the prediction residuals for all observations. AIC (Akaike information criteria) is used to compare various models by determining the relative position of each model's outcomes to the truth.

Beer-Lambert Law Model

Because lidar waves can penetrate forest canopy gaps, it serves as a great technology for understanding how solar light penetrates the canopy. The Beer-Lambert law establishes a relationship between canopy density and light transmission (Monsi and Saeki 2005). It has been used for modeling vegetative canopies, stand densities and stream shading. The Beer-Lambert law was originally written to explain the passage of light through a solution:

$$I = I_0 e^{-kL} \quad (1)$$

Where *I* represents light intensity below the canopy, I_0 is light intensity above the canopy, *k* is the extinction coefficient, and *L* is Leaf Area Index. When a beam of solar radiation transmits through the canopy it interacts with leaves through absorption and reflectance. The extinction coefficient *k* was developed to describe the canopy function in shifting beam radiation. It represents several key elements: canopy clumping, leaf angle distribution, and the type and direction of radiation. Given a known value of *k* one might derive Leaf Area Index (Zheng and Moskal 2009; Breda 2003; Solberg et al. 2006).

If *k* is unknown, an estimate can be used instead, and LAI_E can still be derived. In some ways, Eq. (1) can represent the probability a light beam will permeate through a canopy. An analogy to the relationship of light intensity in this equation can be made using the respective number of canopy and ground point returns of a representative point cloud. So, coupling this canopy/ground return ratio with an estimate of *k* enables us to transform Eq. (1) into:

$$R_g = R_T e^{-kLAI_E}$$

Which can be re-written to form:

$$LAI_E = -\frac{1}{k} * \ln(\frac{R_G}{R_T}) \quad (2)$$

Where R_G is the total number of ground-classified point returns and R_T is the total number of returns. When *k* is being estimated, some studies suggest using a constant 0.05, from a scale of 0.01-0.99. Several variations of *k* were tested against both remote sensing inputs, and best-fit results were very similar in both cases (*See 3.3 Beer-Lambert Model Results*). Readers curious about more underlying details regarding the relationship between the Beer-Lambert Law and ALS are directed to other comprehensive studies (Richardson and Moskal 2009; Zheng and Moskal 2009; Solberg 2006; Breda 2003).

1.2.4 Accuracy Assessment

Ground estimates of LAI_E were made using a Nikon Coolpix 4500 hemispherical camera. The center of each sampled plot was located as close to the original GPS coordinates as possible, but also shifted slightly as needed in order to not be immediately obstructed by small vegetation or a low-hanging tree crown. A tripod was placed at plot center and leveled, holding the camera at 1

meter above ground. One picture was captured and later processed for each respective plot, including additional video footage and annotations to assist in post-processing. For complete details of the field plot sampling regime see Moskal and Cook (2015).

Following Leblanc's (2006) and Richardson's (2010) methodology, These 113 plot photographs were processed with Digital Hemispherical Photography (DHP) software, which partitions each image into 10 annulus rings – each ring representing 9° zenith angle. The most outer rings [10-8] were excluded from the analysis due to the influence of steep topography on calculating LAI_E (which many sample plots in the study area exhibited). This exclusion of the outer rings, paired with the radius of each lidar point cloud cylinder, also aligns with recommended methods found in previous studies (Richardson et al., 2009; Morsdorf et al., 2006; Riaño et al., 2004).

Figure 3. *The image on the left is raw photograph from the hemispherical camera. The image on the right is the visual result of the digital processing used to calculate DHP-LAI_E. Software attempts to categorize "sky", "non-sky", and "mixed" pixels. Users have manual control to adjust spectral thresholds*

Six sample plots were removed from the analysis due to an overwhelming and uncorrectable sun glare present within the hemispherical photo. Three photos had exposed snags with high reflectivity which resulted in the software classifying these as sky. Because of the lack of contrast, these were removed as well. Thus, the final analysis resulted in the baseline estimation

of LAI for 104 total plots. This baseline was used to find the best relationship between each respective plot's conical view of the photograph and its cylindrical lidar metrics (Morsdorf 2006). For more information regarding the procedure of DHP processing and analysis see Appendix B.

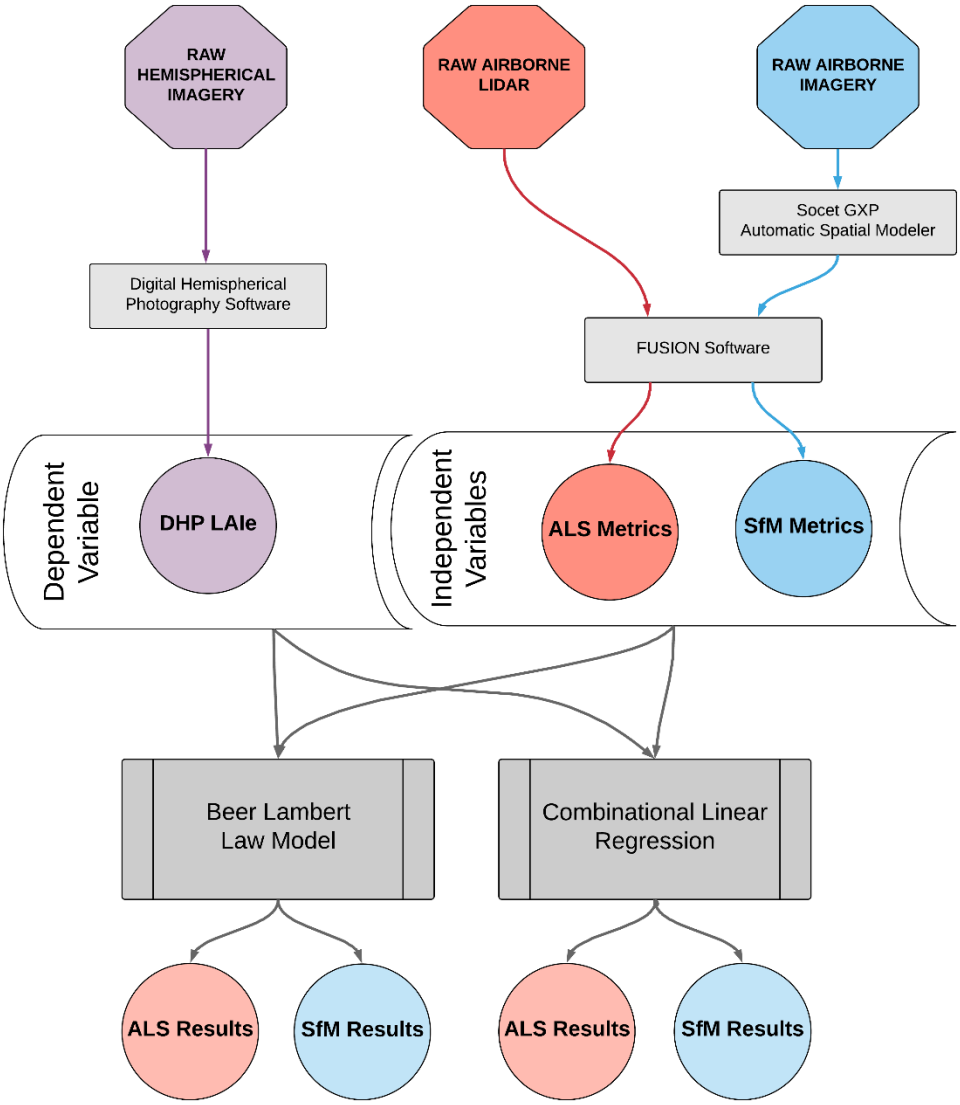

***Figure 4**. A visual workflow of the study.*

1.3 Results and Discussion

1.3.1 LAI_E Estimates

Lidar-based models performed better overall and results indicate a strong relationship between canopy/ground point ratio and DHP-LAI_E, which also validates similar studies (Richardson, 2009; Coops, 2007; Solberg, 2006). Predictive model power was slightly lower than these studies due to the complex terrain and heterogeneous forest types. Performing this technique in homogeneous plantations can yield much higher predictive power (Solberg, 2006).

SfM results did not exhibit this same behavior and performed less well when applied to Beer Lambert Law theory. However, SfM did demonstrate comparable estimates of DHP-LAI_E when using the combinational linear regression, which instead utilized the elevation characteristics of a point cloud: maximum height, mid-range height, and the total covariation of elevation point values within the tree canopy. Additional imagery analysis yielded the grey-level co-occurrence matrix (GLCM). This second-order statistic adds an extra advantage by identifying patterns that occur within a landscape, like the spatial distribution and clustering of trees and canopy gaps (*see* *Further Exploring SfM*). Attempting to add other variables that might be conceptually-explained did nothing significant to alter results.

Model Indicator	Reference	Source Formula	Observations	R^2	RSME
ALS Data Input					
A	Linear Regression	$LAI_E = \alpha + \%R_{C1}$	104	0.66	0.4
B	Beer-Lambert's Law	$LAI_E = \left(\frac{1}{k}\right) * Ln\left(\frac{R_G}{R_T}\right)$	104	0.63	0.44
SfM Data Input					
A2	Linear Regression	$LAI_E = \alpha + \beta_1 Elev.L.CV + \beta_2 Elev.P40 + \beta_3 Elev.P95 + \beta_4 GLCM$	104	0.62	0.4
B2	Beer-Lambert's Law	$LAI_E = \left(\frac{1}{k}\right) * Ln\left(\frac{R_G}{R_T}\right)$	104	0.51	0.44

Table 3 *- Model Results. Performance of modeling approaches to estimate LAI_E against the reference provided by digital hemispherical photography.*

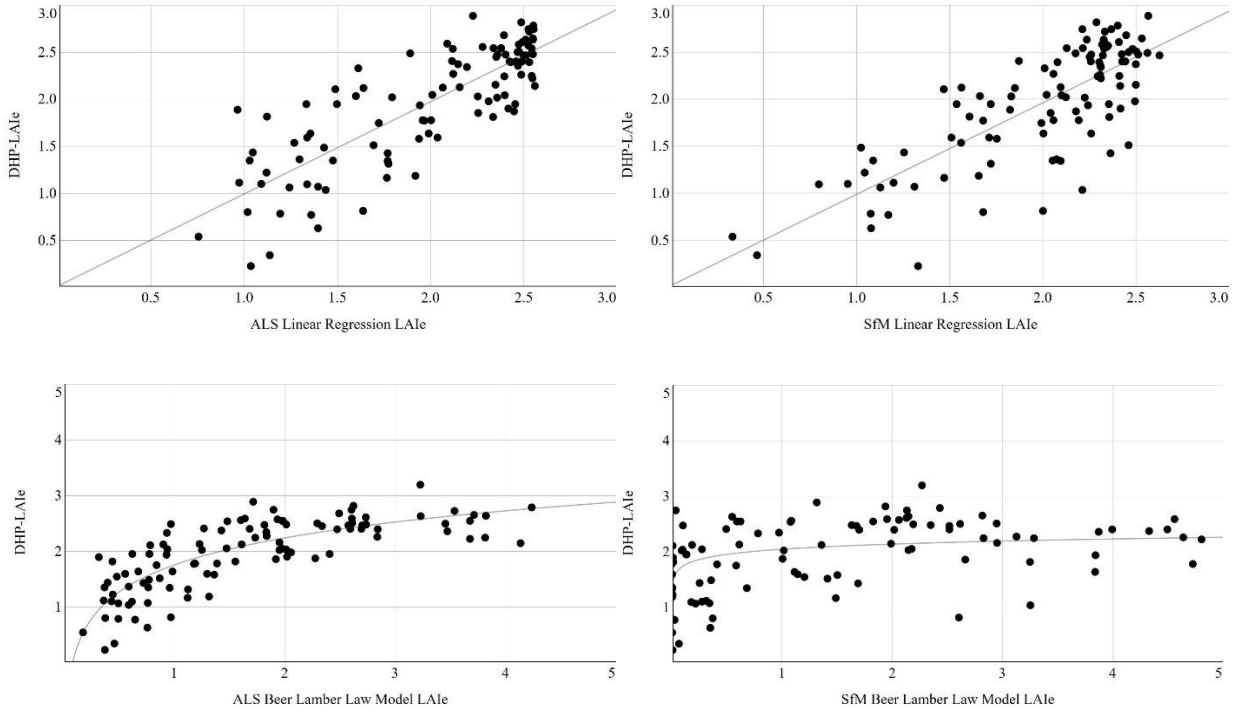

Figure 5 *- All Results Plotted. Performance of modeling approaches to estimate LAI_E against the reference provided by digital hemispherical photography. ALS inputs are on the left and corresponding SfM results are on the right.*

As vegetation overlap increases, so too does the complexity in capturing and quantifying it. The type and heterogeneity of tree-species composition can strongly influence the capacity of remote sensing mensuration. Obscuring factors like terrain and under-story conditions, can significantly affect the accuracy of DHP-derived LAI_E (*see Appendix A.6*). In both these findings and prior studies, remote sensing LAI values have been shown to swell to a point in which saturation occurs. This means that while model-LAI_E estimates may begin to "max-out" at a certain value, real LAI could be much higher (Lim 2003; Riano 2004; Solberg 2006).

1.3.2 LAI_E Combinational Linear Regression Model

Input	Best Model Candidate	R^2	RSME	Breusch-Pagan	RESET	Rainbow	PRESS
ALS	$LAI_E = \alpha + \%R_{C1}$	0.66	0.4	0.0001463	0.7791	0.6165	15

SfM	$LAI_E = \alpha + \beta_1 Elev.L.CV + \beta_2 Elev.P40 + \beta_3 Elev.P95 + \beta_{43} GLCM$	0.62	0.399	0.7157	0.7157	0.6884	18

Table 4 - *Statistical results regarding the final two regression models chosen for each remote sensing input. The only test which shows significance was the Breusch-Pagan for the model using lidar data. This suggests that no final linear model using lidar input was able to avoid heteroskedasticity.*

The two linear models discussed (Model A and A2) are the outcome of a procedure that tests hundreds of combinations of potential explanatory variables in order to find the best-fit linear regression that that describes the DHP-referenced LAI_E. *Table 4* summarizes the results of this process in choosing the best linear regression models for each remote sensing input. *Figure 6* plots the differences in LAI_E estimation for both types of input.

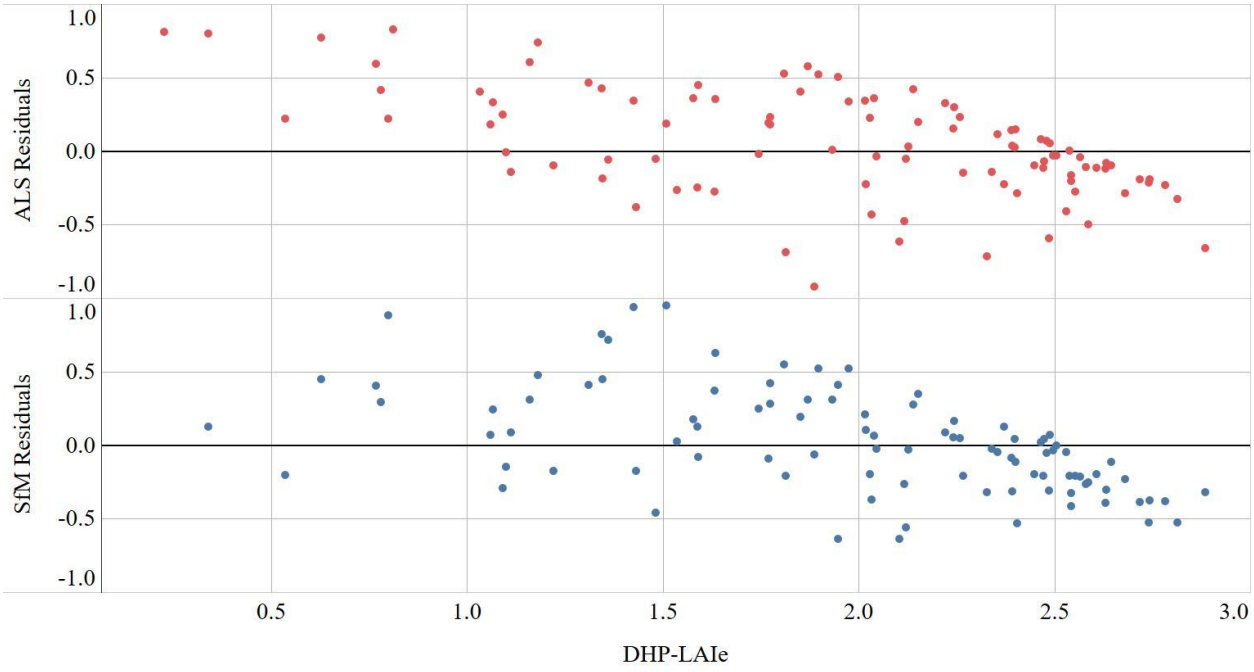

Figure 6. *A comparison in differences of Linear Regression LAI_E estimations between both remote sensing inputs (ALS = red, SfM = blue). Dots align between top and bottom images, corresponding the plot's respective DHP-LAI_E value (x-axis). Differences in estimates represent the y-axis and can be positive or negative.*

ALS Results

The best resulting model from the exploratory-OLS process using lidar data found a strong correlation between ground-measured LAI_E and the percentage of 1st canopy returns, i.e., the total number of 1st returns registered above the canopy/ground threshold elevation compared against the total number of 1st returns. This is represented in equation 1 as $\%R_{C1}$

$$LAI_E = 0.464 + \%R_{C1} \quad \text{(Model A)}$$

While the LAI_E estimates compare to similar studies (Richardson and Moskal 2009; Riano et al. 2004) there are two points of concern with these results. The first is the bottom outlier. If ALS scans indicate all ground points then LAI_E cannot equate to 0.464; it would most likely be much lower, potentially even zero for non-forested landscapes. Second, no light penetration (an extremely thick canopy) has an upper limit of %1st returns = 100 → LAI_E = 2.564. Upper saturation levels of LAI often exceed 3. So, this model struggles under both extreme cases of no forest canopy and extremely thick forest canopy.

SfM Results

The best resulting model from the exploratory-OLS process using SfM data did not utilize canopy-ground ratios of point returns, making it different from the lidar point cloud. This is understandable because the dataset as a whole has relatively far fewer ground returns to work with, and so relies much more on the point cloud's representation of canopy variation. Below is the explanatory-OLS process' ideal model candidate, which will serve as a provisional model for now:

$$LAI_E = 2.439 - (3.998)Elev.L.CV - (0.015)Elev.P40 + (0.014)Elev.P95$$

Where 2.439 is the constant intercept; Elev.P40 is the point elevation corresponding to the 40th percentile height of the entire, respective point cloud; and Elev.P95 represents the 95th percentile height. Elev.L.CV essentially represents the shape of a probability distribution of height values for a respective point cloud. It accounts for effects from the scale, skewness, kurtosis, and standard deviation of all elevation point values for a respective point cloud. The coefficient of variation (CV) element is defined as the ratio of the standard deviation to the mean (Everitt

1998). It is used as a standardized measure of dispersion of a probability distribution or frequency distribution. Elev.L.CV correlates with image texture, which acts as a surrogate for forest structure. Because it is derived from L-moments, it is less sensitive to non-normal distributions. Elevation values of a SfM-point cloud are derived from variations in tone for an individual pixel, which demonstrate a direct relationship with stand-level canopy structure (Wulder 1996).

Further Exploring SfM

Using the spatial information from SfM alone might be undercutting the ability to understand how this technology can be used to assess leaf area. Since SfM is derived from imagery, there is also a spectral component that could be utilized. Plant leaves absorb solar radiation in a photosynthetically active portion of the spectral region and re-emit radiation in the near-infrared (NIR) portion. This allows us to quantify vegetation health by using sensors that capture these specific bands of light, as well as the ones that normally appear in photography. One derived variable used often to assess plant vitality is the Normalized Difference Vegetation Index (NDVI) which is a ratio of the red and NIR spectral reflectance measurements (Rouse et al., 1974). Because the surface area of leaves is directly correlated with how much energy they can potentially absorb and emit, estimating LAI using such spectral responses can be useful (Gong et al., 1992). However, research has shown this is limited to smaller values of LAI (<3) because of the asymptotic relationship between LAI and NDVI: there is a limited variation in NDVI values for LAI values greater than 3 (Wulder et al., 1998). Furthermore, NDVI alone is not capable of estimating LAI: forest-stands of different structures, densities, and canopy cover could ultimately produce comparable values of NVDI because of similar ratios of red and NIR spectral reflectance, despite having disparate values of leaf area.

NDVI represents spectral information that can be associated with vegetation phenomena, while a 3-D point cloud derived from SfM represents the physical structure. However, there is another method in exploring structure, or texture, of an image. In digital image processing, texture is the spatial variability of image tones, which describes the relationship between elements of surface cover, and ultimately changes in the spatial distribution of forest vegetation (Wulder et al., 1998). There are a variety of statics which can characterize tone values between neighboring

pixels. The grey-level co-occurrence matrix (GLCM) is a matrix of relative frequencies which two neighboring pixels occur on an image (Haralick et al. 1973). It calculates second-order statistics using the statistical distribution of local properties and has been applied in other LAI-related research (Wulder et al., 1996).

Average NDVI values for each plot were calculated and plotted against DHP-LAI_E. While NDVI values do indeed show a limited variation in values, they still revealed a very strong correlation with DHP-LAI_E ($p < 0.0001$). It is important to note that many values can be derived from GLCM. Of these, homogeneity, contrast, and entropy were calculated for each plot. The only one to show any statistically significant association with DHP-LAI_E was the value for entropy ($p = 0.013$), which will hereby be referred to simply as GLCM.

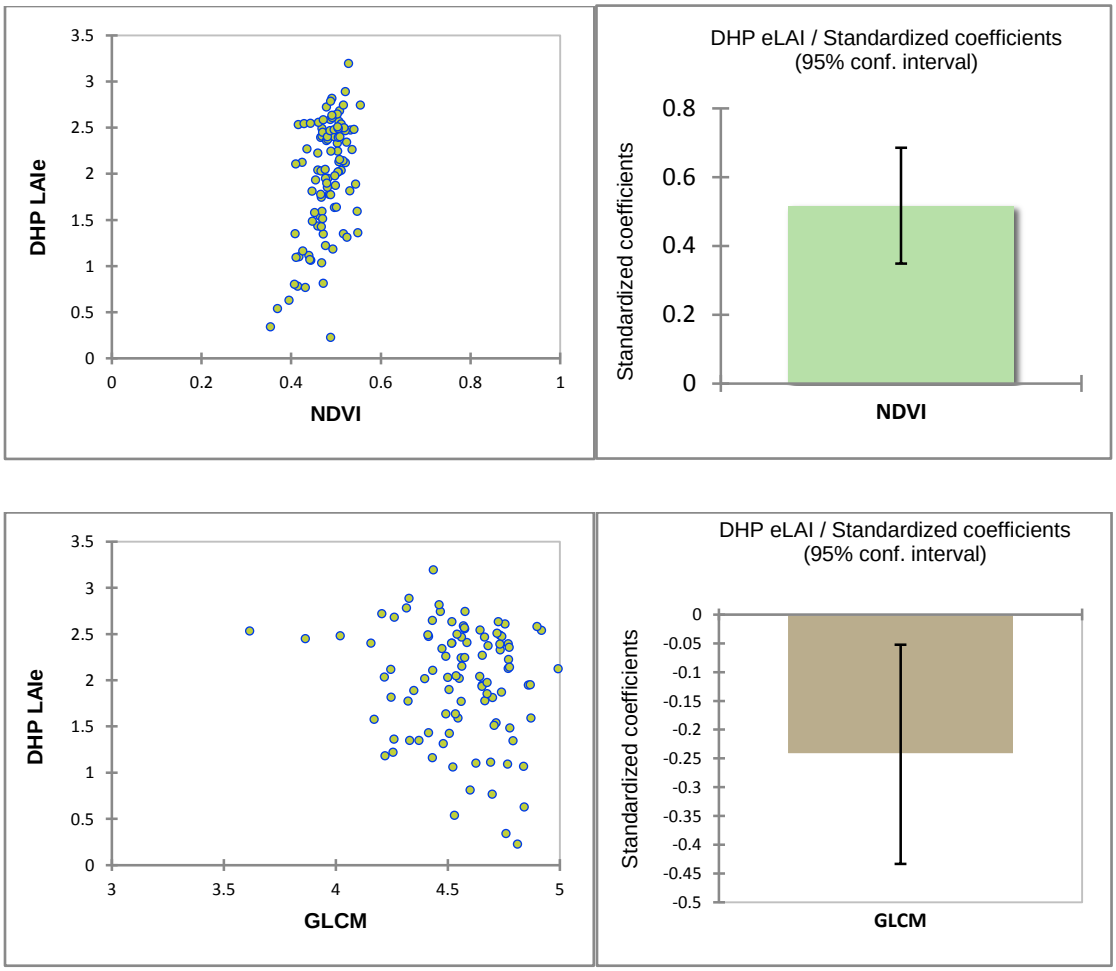

Figure 7. *A visual comparison of NDVI (above) and GLCM (below). Scatter plots show the respective variables when individually assessed against DHP-LAIE values. Bar charts represent the standardized coefficient of each variable when used as a single explanatory variable.*

The two new variables were introduced to the linear model and several variations were tested. NVDI and GLCM alone were poor at estimating DHP-LAI_E but showed promising results when paired with the powerful texture surrogate, Elev.L.CV. Still, this did not perform as well as the original model, probably because Elev.P40 and P95 still capture important sub-canopy elements and general stand height, which have been to show a strong significance when associated with LAI (Monsi and Saeki 2005). Adding GLCM to the original model increased R^2 slightly and decreased RSME, with all explanatory variables showing statistical significance. The addition of GLCM improves the base point-cloud model and does not compromise the predictive power of the other explanatory variables.

$$LAI_E = 4.109 - (4.066)Elev.L.CV - (0.016)Elev.P40 + (0.014)Elev.P95 - (0.358)GLCM$$

Model R^2	0.60	0.618	0.617	0.598	0.505
Model RSME	0.408	0.401	0.399	0.409	0.451
Elev.L.CV	-1.117 < 0.0001	-1.115 < 0.0001	-1.136 < 0.0001	-1.026 < 0.0001	-0.585 < 0.0001
Elev.P40	-1.012 < 0.0001	-1.069 1.72E-04	-1.092 < 0.0001	-0.919 0.001	
Elev.P95	0.922 < 0.0001	0.949 < 0.0001	0.963 < 0.0001	0.864 < 0.0001	
NDVI		0.016 0.852		0.073 0.402	0.147 0.099
GLCM		-0.150 0.027	-0.153 0.018		-0.107 0.143

Table 5. *The results of 5 different iterations of the SfM linear regression model, utilizing two new explanatory variables: NDVI and GLCM. Iterations are represented by a single column, with model results of R^2 and RSME given. Values of the explanatory variables represent standardized coefficients and p-values, respectively. A missing set of values indicates the corresponding variable was not used in that particular model iteration. The highlighted column represents the best performing linear regression model, as applied to SfM.*

Aside from texture, finer spatial resolution can increase the ability to estimate LAI by adjusting the object of interest to leaves. For example, 1-meter resolution imagery is viewing more of a sub-tree object, while a 2 cm resolution is capturing actual leaves. This has been successfully demonstrated using high-spatial resolution imagery from UAVs (Wallace et al., 2016; Chianucci et al., 2015; Matthews 2013). However, employing this technique over a large landscape may not be feasible as this technology is still limited, as are its governing laws. Future research is needed to continue exploring this relationship between LAI-estimation and spatial resolution. Furthermore, the degree of image overlap should be examined; as the number of images per pixel increase, so too does SfM's ability to represent a landscape with finer granularity.

1.3.3 LAI_E Beer-Lambert Law Model

Input	Model	Adjusted R^2	RSME	Canopy/ground Threshold
ALS	$LAI_E = \left(\frac{1}{k = 0.85}\right) * Ln\left(\frac{R_G}{R_T}\right)$	0.63	0.4	1 meter
SfM	$LAI_E = \left(\frac{1}{k = 0.78}\right) * Ln\left(\frac{R_G}{R_T}\right)$	0.51	0.44	Varies

Table 3*. Statistical results regarding the final two Beer-Lambert models chosen for each remote sensing input. Because Lidar point clouds contain for more information associated with ground features it performs much better than SfM in this approach.*

The Beer-Lambert law model that utilized lidar data as input, and a generally higher *coefficient-k* variable, performed better in estimating DHP-referenced LAI_E then the using SfM data as input. Overall, both Beer-Lambert models did not perform as well as their linear model counterparts. Moreover, there is a larger gap in predictive ability between lidar and SfM in using Beer-Lambert models as opposed to an exploratory linear regression on CloudMetrics output. *Table 3* summarizes this information while the proceeding sections explore the results further. *Figure 8* plots the differences in Beer-Lambert LAI_E estimation for both types of input. These figures visually convey that there is more disagreement between lidar and SfM in the Beer-Lambert results compared to Linear Regression results. Furthermore, there is a much higher magnitude in the disagreements; there is a maximum difference of 0 LAI_E = 3 in Beer-Lambert results compared to a maximum of 1 in the linear regression models.

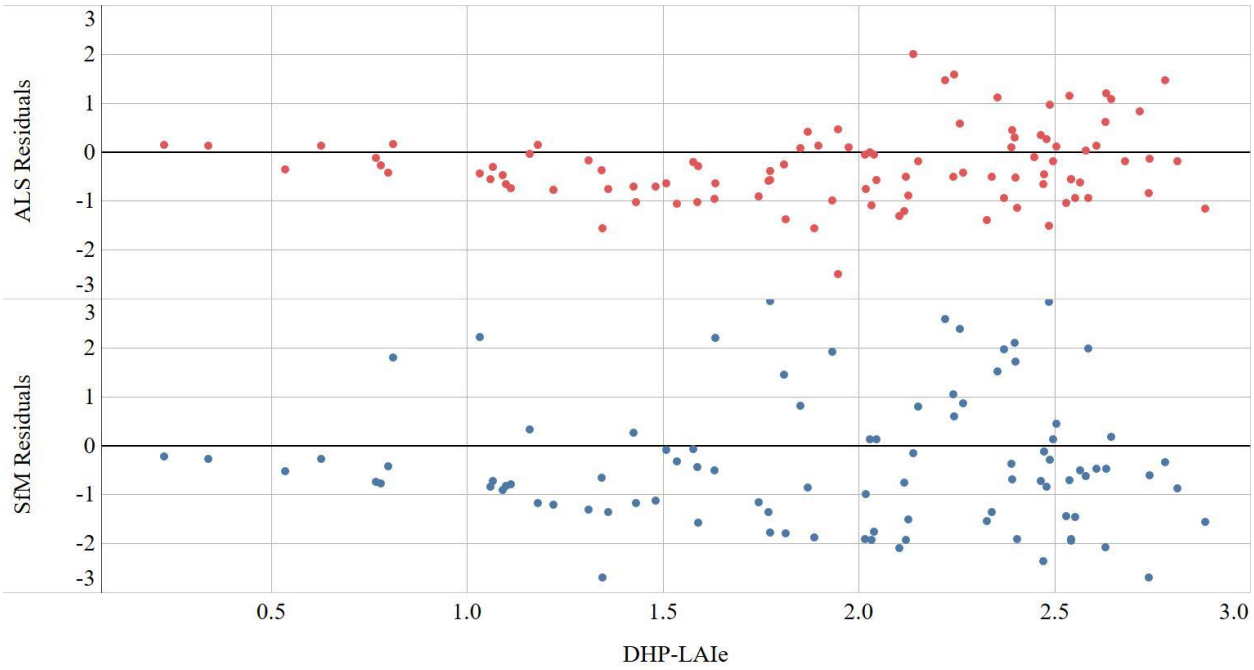

Figure 8. *A comparison in differences of Beer-Lambert Model LAI_E estimations between both remote sensing inputs. Dots align between top and bottom images, corresponding the plot's respective DHP-LAI_E value. Differences in estimates can be positive or negative, and the range of differences vary slightly between input types.*

ALS Results

It is well hypothesized that lidar input for this type of model would perform better than SfM, as far more "ground" data points exist overall in an ALS point cloud due to the laser pulse's high resolution and ability to penetrate forest canopy. Accounting for more granularity of gap sizes within the canopy allows for greater precision in quantifying the relationship of canopy light attenuation. Overall, the ALS-based estimations herein are comparable to studies employing the same technique in similar environments (Richardson and Moskal 2009; Solberg et al. 2006).

There are two limitations in applying this type of model. The first lies in how and how often the values for the *extinction coefficient K* are chosen. In this study, the Beer-Lambert model has a distinct advantage over allometric models, as it is less sensitive to species heterogeneity. But, the variable *K* still represents elements of various forest types (Thomas and Winner 2000; Pierce and Running 1988). Namely, *K* describes leaf angle distribution, radiation type/direction, and canopy

structure/clumping. Some research posits that a range of $K = 0.5 – 0.7$ is suitable for heterogeneous forests as the one used in this study (Vose et al. 1995; Pierce and Running 1988). However, several combinations of tests revealed that higher values of *K* were better-suited for both remote sensing inputs (*figure 10*). Both types of inputs showed the tendency to gravitate to higher values of K, and lower resulting estimation-ranges of LAI_E, in attempting to describe the most variation of the data. This could be a statistical result of K attempting to compensate a generally lower number of ground-classified point returns, which is especially the case in taller more well-established stands. These results align with other studies showing high-saturation points of LAI estimation before accuracy and ability begins to degrade rapidly.

The second major limitation of this method is tied to what it does not estimate: true LAI. The estimates of LAI_E must be corrected to obtain true LAI, which requires multiple correction factors which vary with species. Applying this correction across very large, dynamic landscapes and forest types would not only entail further analyses but would mostly likely require additional reference data.

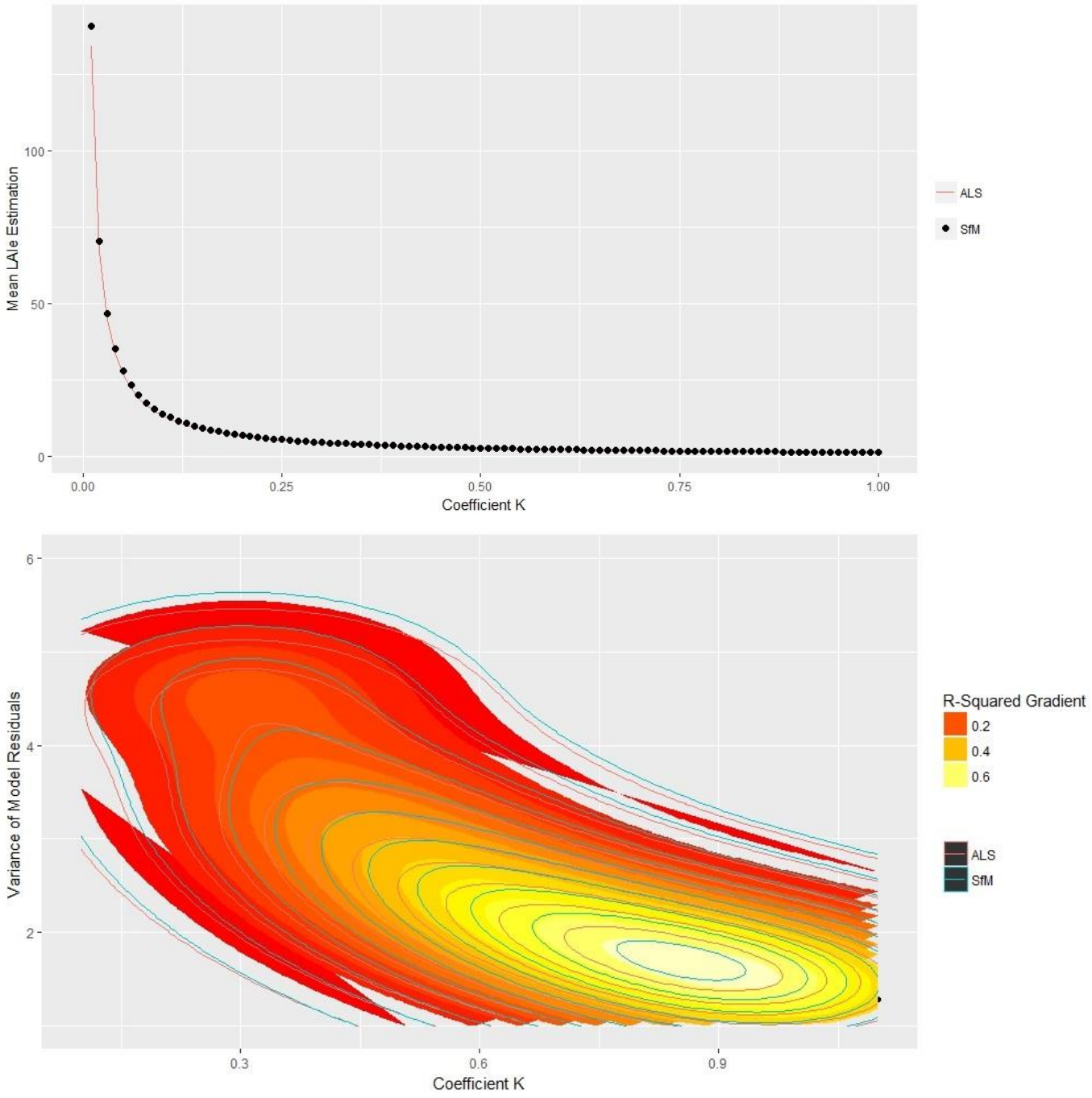

Figure 9. *The two plots above and below visualize the results of a Monte Carlo analysis in adjusting Coefficient K, for each respective Remote sensing input. The top graphic shows the inverse relationship between K and average DHP-LAIE over all observations. Different graphic symbols had to be used for ALS and SfM because both had very similar outcomes. The line shows the* trend *in ALS outcomes, while dots not only represent SfM, but can be interpreted as individual observations. The bottom graphic illustrates how overall model estimation accuracy and its range of* LAI_E *estimation residuals fluctuate with varying values of K. Lower values of K resulted in lower accuracy in estimations, much higher estimates of* LAI_E*, and a much larger variance in error. Outliers of high* LAI_E *estimations for near-zero values of K (mostly in SfM) were eliminated for visual aesthetics.*

SfM Results

These results show that the Beer-Lambert Model performs significantly less well when using SfM data as opposed to ALS data. This aligns with light permeation theory, as discussed earlier: canopy-penetrating light pulses from ALS capture far more sub-canopy elements and thus create a much more rich and dense point cloud than SfM can. However, individual pixels are capable of capturing gaps or dips within the canopy, especially with a finer spatial resolution.

With a NAIP-derived SfM point cloud of 1.3-meter resolution, a varying canopy/ground threshold value, and an optimal, static extinction coefficient, this particular model only could explain just over half of DHP-LAI_E. Similar to the other model variations, this approach suffers both from extreme circumstances of little to no canopy cover to mature and dense forest stands. This model estimated a low LAI_E (less than 1) a total of 50 times, which was much higher than the other models. Of these estimations, only seven of the reference values (14%) were actually less than 1.

Total Estimated LAIe < 1	DHP LAIe < 1	1 < DHP LAIe < 2	2 < DHP LAIe
50	7 (14%)	24 (48%)	19 (38%)

Table 6. *The breakdown of relatively low estimations of LAI_E when using the Beer-Lambert law model and SfM as input data.*

This high occurrence of under-estimating LAI_E might be remedied by employing a more dynamic methodology for canopy/ground threshold specification. Recall Eq. 2: with a very open landscape the number of ground points will start approaching the total number of points, resulting in smaller estimations of LAI_E. These results suggest that varying stages of forest growth seem to be more dependent and potentially associated with the value of the canopy/ground threshold. Whereas ALS-derived results all correlate well with a constant threshold tied to the same elevation as the reference data, SfM-derived results indicate the need for a more advanced approach. Perhaps tailoring the canopy/ground threshold for each individual reference plot based on that plot's structural characteristics might produce more accurate results, but it would come at the cost of introducing a very complex and time-consuming step to the existing workflow.

There was also a logarithmic trend of over-estimation with a few outliers. Seven of these were isolated and compared. There was nothing similar about species composition or geographic location but it was evident all were composed of very large trees. For the seven plots, the average DBH = 45 cm (18 in.), average tree height = 28 m (93 ft.), and average crown diameter = 7.3 m (24 ft.). While larger and more mature forest stands would indeed gross a larger volume of tree canopy over time, there seem to be certain strata of forest growth types that affect the SfM approach differently. These results suggest that forest size and age must be taken into consideration when adjusting inputs for SfM-based Beer-Lambert model. Further research is needed to define exactly what these are, but other models may prove more fruitful for SfM technology as its ability to produce a higher number of ground points is limited.

Chapter 2: The Societal Value of Remotely Sensed Ecological Information

Travis Axe, 2018

2.1 Introduction

At the turn of the 21st century the United Nations sanctioned the Millennium Ecosystem Assessment (MA) to "assess the consequences of ecosystem change for human well-being and the scientific basis for action needed to enhance the conservation and sustainable use of those systems and their contribution to human well-being" (Millennium Ecosystem Assessment, 2005). The assessment spanned four years and involved over 1,000 scientists and experts from almost 100 different countries. It concluded that ecosystems have recently contributed to substantial net gains in economic development and human well-being, but also that society has changed ecosystems more rapidly and extensively in the past 50 years than in any other time in recorded history. This has induced largely irreversible loss in the diversity of life on Earth. Significant changes in policies, institutions, and cultural awareness could enhance certain resource environment services and longevity, but if left unaddressed, potential benefits will be diminished for future generations and will threaten the well-being of human and natural populations.

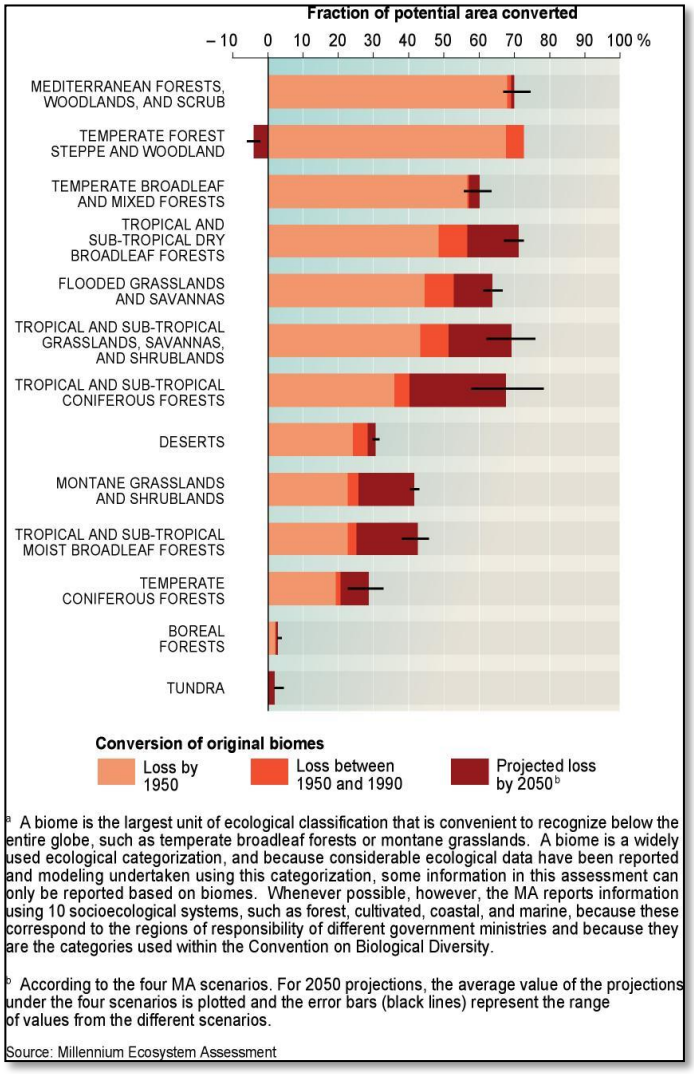

When all the benefits derived from the environment are not entirely or accurately represented in economic transactions, then ecosystem changes that impact the health and well-being of society arise. Thus, there exists unmet opportunities to expand our ability to both capture and better understand these values (Barbosa et al., 2015; People and Pixels, 1998). As the MA concludes, failing to do so could result in declines in resource environment

supplies and quantities, and subsequently in social welfare. Mankind's largest impacts on the ecosystem result from ever-growing demands for food, water, timber, fiber, and fuel (Millennium Ecosystem Assessment, 2005).

Remote sensing technologies can bolster the economic analyses and the subsequent policies needed to sustain these needs by providing more frequent, accurate, and comprehensive information representing the values that the environment bestows (Brouwer et al., 2015; Freeman et al., 2014). For decades remote sensing has offered unique advantages over traditional natural-resource mensuration: the ability to cover large areas, acquire multiple captures over time, allow for precise measurements, and ultimately provide valuable information for studying mankind's interaction with the environment (People and Pixels, 1998). There is demonstrated value for remote sensing technology to enhance natural resource management, and many opportunities continue being experimented and explored (Casu et al., 2017; Wang, 2013; Rindfuss et al., 2012). But challenges exist in readily transforming remotely sensed data into information valuable to natural-resource managers and social scientists.

First, many of the variables used in social policy research are abstract and cannot be readily captured from remote sensing platforms (Ex: income, years of education, family size, age, etc.). Tangible objects like land-use change and building construction can be quantified via remote sensing, but it is important to remember these are only the materializations of land-tenure laws, government policies, and market mechanisms: all primary interests to social scientists. Second, there exists a knowledge gap between remote sensing scientists and social scientists. Disparate theory, methods, and jargon exist within each respective discipline (People and Pixels, 1998). Thus, incorporating remote sensing into higher-level policy not only requires a fusion of data, but also an important bridging of scientific tradition (Barbosa et al., 2015).

Scientists are generally aware of the utility remote sensing can provide in social investigation; as physical changes in urban populations and natural ecosystems can be viewed over time through aerial or satellite imagery (Eigenbrod et al., 2010). Yet many remain unaware of the byzantine process required to translate photographs of the Earth into accurate, scientific or economic information that is readily applied to policy-making processes (Barbosa et al., 2015). Moreover, capabilities are becoming more specialized and inexpensive due to investment and development

in sensor and computer processing technology (Kennedy et al., 2009). Indeed, distilling the key technical concepts from a remote sensing study or application can be challenging for a non-expert. However, remote sensing scientists can take measures to bridge this gap. While most environmental remote sensing reviews focus on evaluating sensor types and analytical methods for quantification or change detection, few elaborate on how results may be applied in long-term management goals; specifically, the relevant capabilities, assumptions, and constraints required to understand what long-term monitoring capability is feasible (Kennedy et al. 2009).

This chapter is for researchers and practitioners who have limited understanding in how remote sensing science may be applied to environmental policy and create value to society. It is for those who wish to begin establishing the foundational knowledge required for bridging the gap between remote sensing science and social science. This requires, at the least, a general understanding of how environmental issues are translated into and affected by economics (Keohane and Olmstead, 2016). This chapter provides a discussion that one can utilize to better understand the societal value of the operation and policy application of the scientific information provided by remote sensing technology. The discussion will cover three major points:

(1) A primer on the ways in which society values the environment and how these values may be perceived and quantified, and the dynamic behavior that exists between them.
(2) A major policy tool used in quantifying these values, Benefit Cost Analysis, and why it is useful for framing environmental issues and how remote sensing can contribute to its outcomes.
(3) Remote sensing applications used to increase our understanding of society's interaction with the environment.

2.2 The Exchange of Value between Society and the Environment

In order to better understand how remotely sensed, ecological information can contribute to decisions in environmental policy, the following must first be understood: different types of people value the environment differently. Some of this value is directly monetized and traded, while some is not. Either way there is a shared, comprehensive, and ongoing exchange of value between society and the environment. The word *value* holds disparate meanings to ecologists and economists. Ecologists perceive something that possesses inherent quality and is worthy for its own sake as valuable (Freeman et al., 2014); economists would interpret something valuable more akin to "a commodity or service that is useful to man but that must be paid for."[1] This difference in perception stems from a varying philosophic distinction of value: intrinsic value and instrumental value. Intrinsic value is something that is esteemed for its own qualities; its value is not derived from utility. Conversely, instrumental value is something useful because it serves some other end or purpose (Freeman et al., 2014).

Whichever way value is perceived, the most important environmental issues to humanity are inextricably bound to human behavior, so being able to measure environmental features in a way that is comparable to other issues is paramount. Moreover, all economic activity is ultimately based on resources found within this world, and because of this, we must create a common yardstick in which social and ecological issues can be measured. Ultimately, this means valuing the environment via economic monetization (Keohane and Olmstead, 2016).

2.2.1 The Resource Environment

Ecology and economics are both complex disciplines with uncertainty embedded between scientific findings, market behavior, and real-world, ecological phenomena. Thus, drawing firm and logical connections between all the types of value society derives from the environment is no easy feat. As with many complicated subjects, it helps to simplify things by utilizing common

[1] *Webster's: Ninth New Collegiate Dictionary.*

themes or characteristics. For the environment, we can define values by examining how they interact with and affect society (Van Zyle, 2014). Does an environmental value require the physical consumption of resources? Are resources completely exhausted in the process? What values arise from the existence and non-consumption of resources? What about future values? For discussion, consider a resource environment as the flow of all environmental resources, functions, and services that directly and indirectly benefit, and interact with, mankind (for any relevant issue/population/ecosystem).

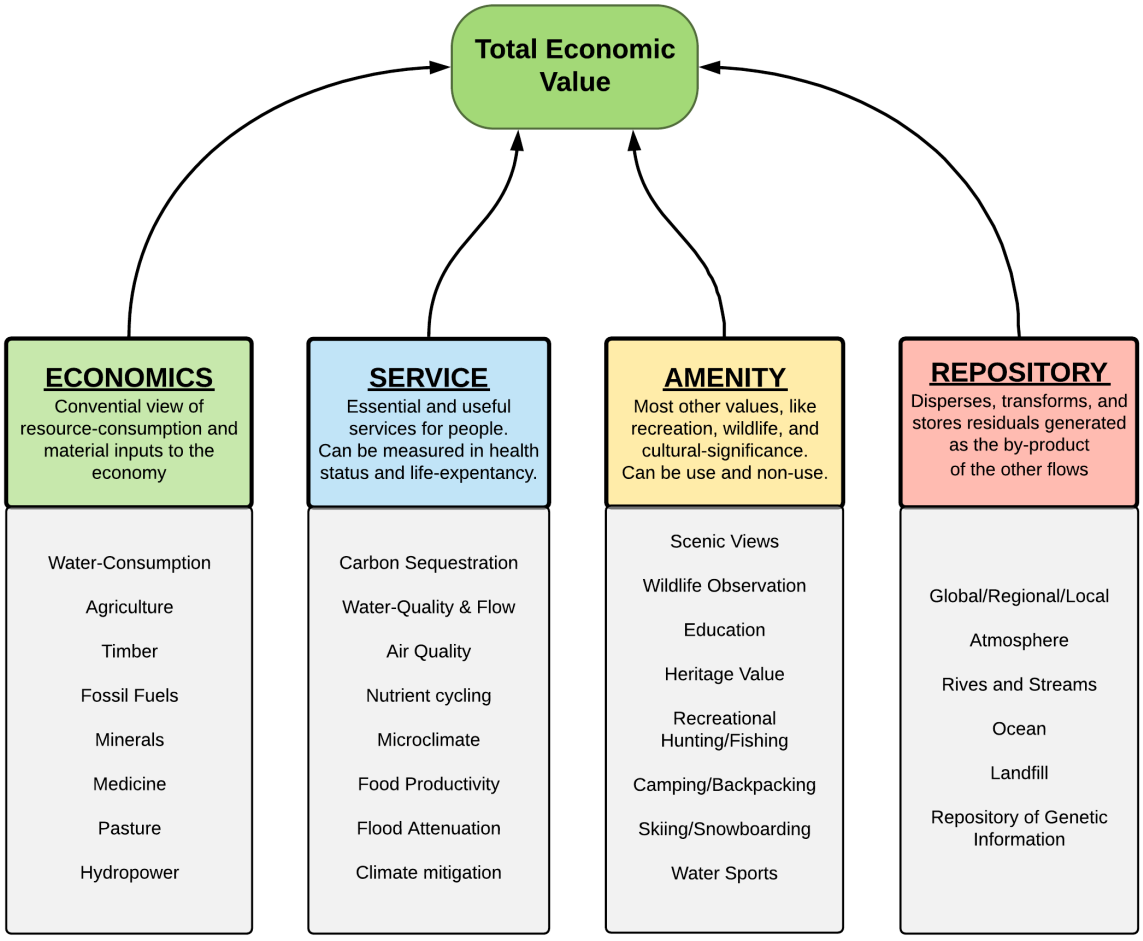

Figure 10. *A visual depicting the main elements of the resource environment. Examples of values are included for each major type but are not considered to be exhaustive set. Source: adapted from Freeman (2014), with modifications by the author (Axe, 2018).*

The values composing the resource environment can be categorized into four major flows.

(1) Economics: The first major value flow of the resource environment is the most directly translatable into economic markets. It is the monetary reflection of natural resource consumption and use and usually has the most well-represented market prices among all types of values. (2) Service. The second flow benefits mankind more indirectly, with some elements serving as essential life-support functions. (3) Amenity. The third flow of values represents mankind's spiritual, cultural, and athletic relationship with the land. (4) Repository. The final flow of values is derived from a system that disperses, transforms, and stores residuals generated as the by-product of the other flows. This also serves as the repository for genetic information that helps determine the stability of the system in the face of anthropogenic and other shocks (Freeman et al., 2014)

2.2.2 Dynamic Interactions of a Resource environment

The benefits and consequences of a resource environment experienced by society are spatially-dependent on the given environment, so it's imperative to understand the various stakeholders within this social framework of exchange. Ex: A national park could provide value to a variety of people, many of whom do not reside within close geographic proximity. However, a polluted water basin from an old mine places consequence almost entirely on the populations dependent on that water basin. In any case, the exchange of costs and benefits between a variety of societal stakeholders and ecological systems is dynamic and unique (People and Pixels, 1998). Moreover, if a policy favors certain benefits from one service flow the net value of that flow will increase, while potentially decreasing value from other service flows. Ex: A policy may set standards for the width of riparian forest buffers around major streams. The height, density, and width of riparian vegetation directly affect the attenuation of solar radiation, so regulating buffer widths in turn regulates stream and soil temperature, stream and soil quality, wildlife and fish habitat, and flood/erosion resiliency (Dewalle, 2010). A larger forest buffer could mean an increase in the value of ecosystem services and amenities and an improvement in the economic flows of fish habitat and population. However, this in turn could decrease potential economic benefit for the timber industry, both from unrealized revenue and operation costs. It could also place more discretionary-restrictions on private-land owners (Freeman et al., 2014).

Whichever values a particular policy may advocate, it remains that any change in resource flows, whether benefits, costs, or damages, will have its own counterparts within the resource environment system. Successful governing entities of natural resources must be able to facilitate this exchange, and understand the incentives, values, and risks that exist for all stakeholders. A relevant economic analysis used for the application of environmental issues is benefit-cost analysis (Helm 1996). Benefit Cost Analysis (BCA) is a useful framework that can assist an analyst in organizing and expressing certain kinds of information through a prescribed set of procedures. It strives to represent the dynamic behavior of resource environment flows in response to a certain policy, by listing all potential outcomes of relative values as either benefits or costs. Finally, it is useful for the purpose of this paper as a BCA can provide remote sensing and environmental scientists a high-level framework for conceptualizing how the values of different environmental policy solutions are compared. From here, a link can be established between the BCA process and the contribution of remotely sensed ecological information.

The next section outlines the fundamental structure of BCA, posits why it is an important tool for addressing environmental issues, and highlights where in the process remote sensing creates value. It will highlight elements of this tool and explain how they are supplemented and supported by remote sensing technology. There are also many studies that have explored and demonstrated the societal value of remote sensing and are not directly associated with a BCA (Casu et al., 2017; Brouwer et al., 2015; Wang, 2013; Rindfuss et al., 2012; People and Pixels, 1998).[2]

[2] Some important economic theory used in evaluating BCA is beyond the scope of this section. (Ex: demand and supply functions, consumer and producer surplus, deadweight loss, stated and revealed preferences, etc.) For a detailed understanding of microeconomics, welfare economics, and the subsequent implementation of a Benefit Cost Analysis, readers are encouraged to pursue more exhaustive guides (Keohane and Olmstead, 2016; Boardman, 2014; Helm, 1996).

2.3 Comparing Values using Benefit Cost Analysis

United States Executive Order 12291 (1981) mandates that all new major regulations be subject to a Benefit-Cost Analysis (BCA): "… regulatory action shall not be undertaken unless the potential benefits to society for the regulation outweigh the potential costs to society [and] regulatory objectives shall be chosen to maximize the net benefits to society…"[3] BCA is a useful tool within environmental policy because it seeks to maximize the net benefits to society and potentially bolster practices that promote ecological sustainability (Keohane and Olmstead, 2016). BCA is grounded in welfare economics and helps decision makers improve social welfare by providing important, monetary calculations behind potential outcomes. Therefore, systematically understanding how a policy influences the benefits, costs, and trade-offs of resource environment flows can improve our ability in addressing environmental issues (Helm, 1996).

Remote sensing can improve the integrity of a BCA by supplementing the knowledge base of a resource environment and its social counterparts. It can provide additional data and supplement methods used in valuating environmental resources and processes. This ensures all those who have standing in an environmental issue are represented, and their values accurately reflected. By offering precise, spatially continuous, and frequent observations, remote sensing yields information that enhances our understanding of ecological quantities, processes, and the subsequent interactions with social systems (Barbosa et al., 2015; Brouwer et al., 2015; Freeman, 2014; Palacios-Orueta et al., 2012; Muraoka and Loizumi, 2009).

2.3.1 BCA Fundamentals

A BCA measures economic efficiency: how well resources are deployed in their highest valued uses. Economic efficiency in a BCA corresponds to maximizing the difference between total benefits and costs. Through the framework of BCA, a good policy will maximize aggregate societal wealth. Although each BCA will emphasize and reflect certain elements depending on

[3] *46 FR 13193, 3 CFR, 1981 Comp., p. 127, Section 2., Parts B and C*

the situation being addressed, almost all will exhibit the steps listed in *Appendix F* (Boardman, 2014).

BCAs consider the potential value of outcomes over time and compare alternatives with one another. The inputs are viewed as opportunity costs and the outputs (or benefits) as willingness to pay. Willingness to pay (WTP) can include things like: how much society would pay to avoid an environmental risk or what someone would pay for an acre of land, a backpacking permit, or a pound of salmon. It can also represent how someone's willingness to accept compensation to forego change (ex: not felling trees on privately-owned forest). Opportunity costs are the value of goods and services that would have been produced had these resources been used instead in the best alternative way. These include raw-material inputs, labor, public-expenditures, unrealized revenues, leisure-time spent, etc. Net Benefits are rendered by subtracting net opportunity costs from net WTP (Boardman, 2014; Freeman et al., 2014).

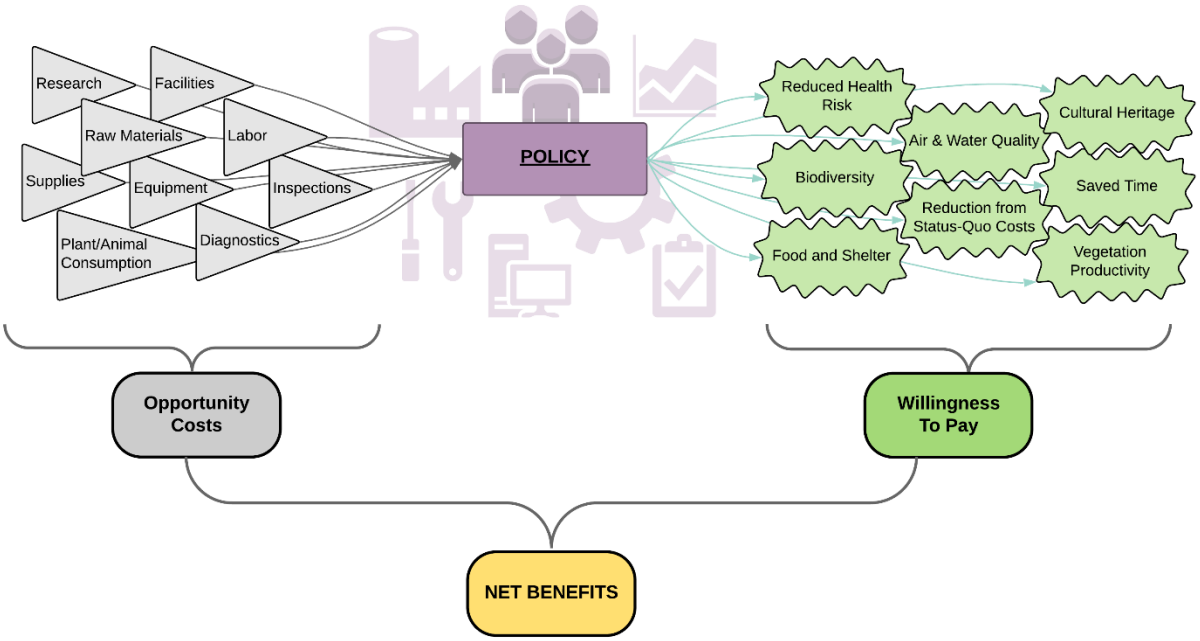

Figure 11. *Categorizing the Net Benefits of a Benefit Cost Analysis with various examples. Opportunity costs measure the value of what society must forgo to use the input to implement the policy. Willingness To Pay represents the benefits each person would have to receive under the policy so that he or she would be indifferent between this and the status quo. The sign of net benefits indicates whether it would be possible to compensate those who bear costs sufficiently so that no one is made worse off and at least one*

person is better off. Positive net benefits indicate the potential for compensation. Source: adapted from Boardman (2014), with modifications by the author (Axe, 2018).

2.3.2 An Opportunity for Value

BCA is a relevant tool for comparing policies because it attempts to consider all the benefits and costs of a resource environment experienced by society as a whole. But an inherent weakness exists: if not all relevant benefits and costs are properly represented and valued then outcomes of the analysis could differ greatly from reality and undermine a policy's ability to address the issue (Boardman, 2014).

Calculating the monetary value for resource environment benefits usually depends on the specific service flow. Ex: Economic services are most often well-reflected in market transactions, where amenity services might need to be estimated by using market proxies or survey techniques. The total WTP for any resource environment value can be generated from multiple valuation methods, so analysts must exercise caution when aggregating values because of potential overlap (Brouwer et al., 2015). This differentiation also ensures that the benefit of each distinct ecosystem condition or process, to each human beneficiary, is counted only once. But valuation methods carry a great deal of uncertainty, and there has yet to be a unanimous agreement on a single classification scheme and valuation method for a resource environment (Wallace, 2007). The scope of this paper is not to explore the intricacies of these valuation methods, but to note them as a crucial step within BCA, as well as to indicate that remotely sensed information is capable of supplementing and refining them. For detailed information regarding valuation methods readers are encouraged to pursue more exhaustive guides and tools (*see Appendix E*).

The economic value of a system of environmental resources is the sum of the discounted present values of the flows of all the services. But many of these services are not bought or sold in markets and do not have market prices, so the economic value of the service may be different from its market value (Freeman et al., 2014). For example, a hectare of forest land could be valued based on potential timber sales, which are set in a well-functioning, competitive market. However, its value might be different if the benefits of other ecosystem services like wildlife

habitat, carbon sequestration, and soil recharging are accounted for. Unfortunately, the actual prices for these services are usually not readily available, have higher uncertainty, and are often underestimated (Freeman et al., 2014).

This can be problematic because the true economic value may be underrepresented by the actual market value and excluding environmental considerations in economic markets can result in negative externalities (Freeman et al., 2014; Helm, 1996). Examples include deforestation, loss of wildlife, decreased water quality, loss of food productivity, and atmospheric pollution. The inclusion of all values derived from a resource environment has been shown very difficult to render given a variety of reasons, both scientific and ethical (Helm 1996). But without monetarization there can be no base for comparison. So, despite many values being difficult to measure, or natural features seeming "priceless," there is still incentive to monetize them so they may be utilized by economic tools used in decision-making (Keohane and Olmstead, 2016).

2.4 How Remote Sensing Creates Value

2.4.1 Primary Applications

Most remote sensing applications utilize radiation reflected off the earth's surface, either solar or instrumental, to estimate ecological changes over time. It can use direct measurements to estimate properties or indirectly infer other properties through contextual relations (People and Pixels, 1998). The resource environment service in question will drive what sets of information are needed to render an accurate monetary value. This could be anything from energy production to soil formation.

One of the most wide-spread and well-used applications is using land cover classification as an input of resource environment valuation. Remotely sensing captures the evidence of major forces like urbanization, agricultural expansion, deforestation, and road development. Land cover is broadly calculated based on pixel-classification and spatial size (Eigenbrod et al., 2010). Assuming that the total resource environment value is scaled appropriately to the respective remote sensing specifications, it remains that this valuation technique is highly influenced by the chosen spatial, spectral, and temporal resolution. This can be problematic with coarser resolutions, as large classes can be overestimated, while small or rare classes are subdued (Cai et

al., 2013; Nelson et al., 2009; Doan and Foody, 2007). However, this particular niche of research is still emerging, and evolving technology could drastically improve results. As computer processing, machine-learning, and remote sensors increase in sophistication and decrease in price, the ability of land cover approaches to more accurately represent resource environment services will too evolve (Cabello et al., 2012; Zinnert et al., 2011).

Remote sensing can play an important role in understanding and regulating water and air quality. Water characteristics that are used in treatment and purification, like chlorophyll-a, dissolved oxygen, and turbidity, are associated with natural radiation absorbance, which can be detected in passive remote sensors (Spillman et al., 2007; Asner et al., 2004). Object-based classification of satellite imagery has demonstrated abilities in tracking the dynamic changes of semi-arid wetlands overtime and projecting their future behavior (Halabisky et al., 2011). Air pollutants can be detected from spectral variation, and when combined with simulation models, help to characterize and regulate air quality (Mozumder et al., 2013; Roots et al., 2011; Chu et al., 2003).

Vegetation indices have been a major element in exploring remote sensing's ability to monitor vegetation health and production. NDVI, EVI, fPAR, and LAI all take advantage of the relationship of between photosynthesis and spectral reflectance. They have been demonstrated to quantify and map forest composition, growth, yield, biomass, and biodiversity (Babcock et al., 2017; Prabakaran et al., 2013; Vaughn et al., 2012; Wardlow and Egbert, 2008; Kastens et al., 2005; Moskal et al., 2004). These indices could also aid in the creation of new value, as their close relationship to net CO^2 flux could spur acceptance and support functionality of carbon markets (Kross et al., 2013; Hao et al., 2012; Potter et al., 2008).

Lidar and Structure-from-Motion methodologies can describe forest canopy structure and volume, which provide value to several types of resource environment services. One example of a promising ecological indicator is LAI, because it interconnects with multiple ecological processes and can be scaled without sacrificing information integrity. LAI is a measure of surface area, so it serves as a proxy for measuring the amount of solar radiation that permeates through a canopy. This light penetration determines the types of understory vegetation capable of growth and affects wildlife habitat. Possessing this type of information across a forest, managers

can better understand effectiveness of silviculture methods and utilize additional insight for mitigating wildfire severity (Littell et al., 2016). Solar light penetration also directly affects wildlife and fish populations by affecting air and soil temperature (Jennings, 2017). Another key advantage of LAI is its consistency through spatial scale changes, which makes it even more meaningful as biophysical parameter for multi-scale research (Zheng and Moskal, 2009).

Remote sensing has also demonstrated value in supporting food production by contributing to our capacity to quantify, map, and predict crop yields (Mkhabela et al., 2011; Drolet et al, 2008; Fuller, 1998). Moreover, analyzing indices like non-photosynthetic vegetation and green vegetation and processing them through a spectral mixture analysis can estimate soil fertility (Liu et al., 2013a; Numata et al., 2003). Studies that combine vegetation indices with other data from surveys, market sales, and social studies, offer additional insight into the relationship between land-use and ownership in areas like agriculture, forestry, and urbanization (Wang, 2013; People and Pixels 1998). When integrated with social science data, remote sensing can quantify and map variation in resource environment services. Techniques like urban sprawl analysis, econometrics, historical data, socio-economic meta-analysis, and stochastic and multi-agent models have shown promise in characterizing how services vary over time with changing social constructs (Linard et al., 2013; Frank et al., 2012; Evans and Kelley, 2008).

Some studies have sought to explicitly determine the value of remotely sensed information by quantifying the benefit of having it available to decision-makers, versus a situation where it is absent. The remote sensing input is considered a unique technological innovation that, when applied to improve on a current land-use allocation, creates an outward shift in the regional production possibility frontier (PPF). The value of information for the remote sensing input is derived from this PPF shift (Bernknopf, 1997).

2.4.2 Synthesis of Research

Barbosa et al. (2015) evaluated the integration of remote sensing technologies into resource environment concepts and practices by synthesizing all studies on ecosystem services between 1960 and 2016 and identifying which studies framed their work in the context of spatially explicit remote sensing assessment. The studies addressed resource environment services as either the main or secondary subject; contained “ecosystem services,” “ecological services,”

"environmental service," "remote sensing," or "earth observation" as keywords; were published in scientific peer-reviewed journals; and were written in English. The criteria initially located almost 6,000 studies, but only 211 of these (~8%) directly utilized remote sensing as a tool or method. However, remote sensing only entered mainstream ecosystems services research in 2005, which also coincides with the Millennium Ecosystem Assessment publication.

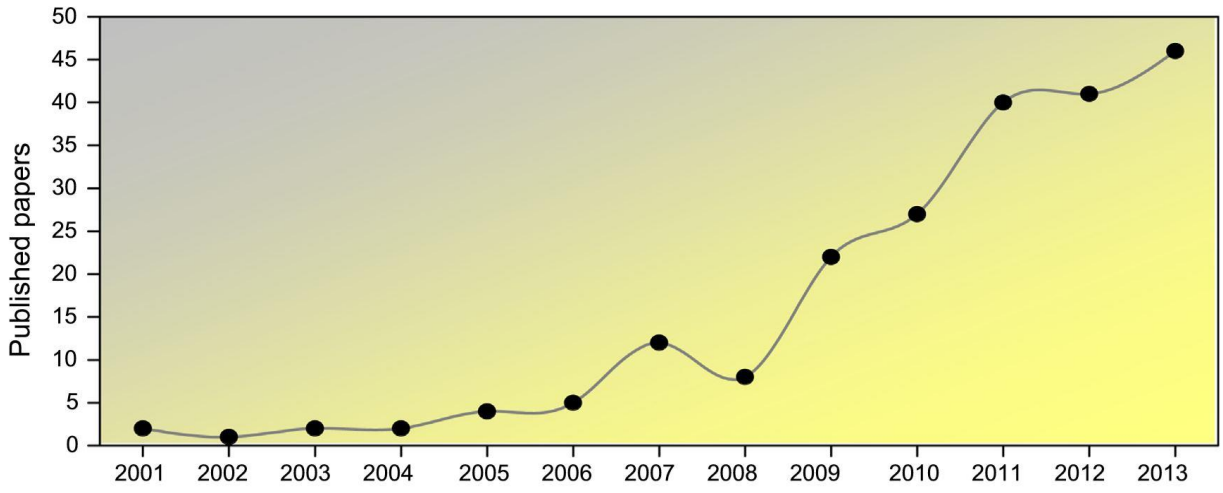

Figure 12. *Number of papers published annually between 2001 and 2003, representing only research which integrated remote sensing into the explicit context of ecosystem services research.* Source: Barbosa et al. (2015).

The primary ecosystem services and remote sensing variables were chosen based on both findings of the synthesized research and MA guidelines (Millennium Ecosystem Assessment, 2005) These results were re-coded to reflect the resource environment framework referenced earlier and are shown in Figure 18. For supplemental information and additional results see *Appendix G*.

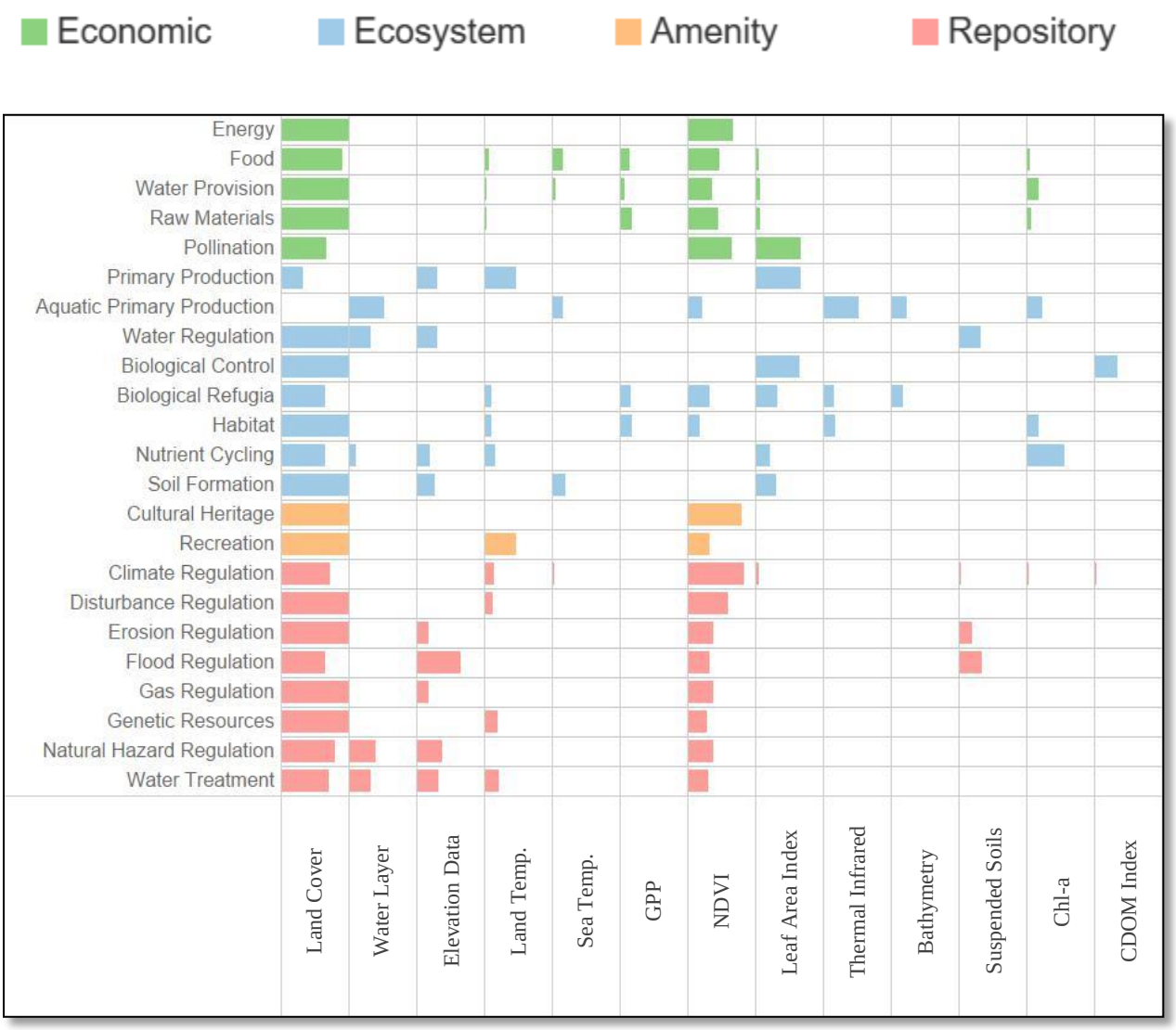

Figure 13. *Percentage of publications that directly utilize remote sensing to assess resource environment services, categorized by respective service flow. Rows represent services, and columns represent remote sensing variables. The width of each column signifies the percentage of publications, for a respective service, that utilized a given variable (the maximum adjusted to 50%). Publications represent 211 distinct studies spanning 1960-2016.* Source: adapted from Barbosa et al. (2015), with modifications by the author (Axe, 2018).

The results clearly suggest that land cover and NDVI were the primary remote sensing variables used in assessing almost all resource environment services, while others like elevation data, land

temperature, and LAI being were used frequently, but in more specific cases. There is also a trend revealing that ecosystem-based services explored a wider use of remote sensing variables compared to other services. Some key findings of the systematic review indicate that remote sensing does contribute to a variety of resource environment services, it may only be practical when two things are first understood: (1) key interdependencies and behaviors within social-ecological systems and (2) the nature of the relationship between remotely sensed data and the service of interest (Barbosa et al., 2015). Finally, the review reveals remote sensing's relatively small footprint in this type of research and suggests that many opportunities still exist for bolstering the understanding and management of resource environment services. Indeed, remote sensing's ability to add value in the relationship between mankind and the environment is far from being fully realized.

Conclusion

This study used a two-pronged approach for investigating how the science of remote sensing creates value when integrated into environmental concepts and practices. First, it demonstrated that SfM has a comparable ability to ALS for estimating LAI_E, even in complex forest stands. This bolsters evidence that SfM could be employed as an inexpensive and potentially viable alternative to ALS for quantifying a high-value indicator associated with many ecological processes. Second, the study revealed that remote sensing technology, as an applied tool for directly supporting ecosystem services, is still in its infancy. Research recently started emerging at the turn of the century, and most research-applications only utilized simple land use cover or NDVI indexes to support decision making. As sensors and acquisitions become more inexpensive, and computer processing becomes more powerful, opportunities to incorporate remotely sensed ecological data into higher level decision making will become more feasible.

But there are important factors that must be accounted for in order for remote sensing to be successfully applied. It is paramount for decision makers and researchers to firsts understand the key interdependencies and behaviors within social-ecological systems and the nature of the relationship between remotely sensed data and the service of interest. Moreover, the specifications of the research problem must align closely with the specifications of remotely sensed data to increase the value of data. For LAI, imagery containing a much higher spectral resolution can provide the granularity needed to capture the relationship between vegetation productivity and subsequent energy reflectance. So, being able to measure the portion of the light spectrum that plants reflect in a finer scale can help fine-tune estimations of foliage presence, size, and productivity.

Remote sensing shows great potential to improve the integrity of decision making processes for environmental issues. By offering precise, spatially continuous, and frequent observations, remote sensing yields information that enhances our understanding of ecological quantities, processes, and the subsequent interactions with social systems. This warrants more research that continues to explore the accessibility and affordability of remote sensing applications.

Appendices

Appendix A: Reference Data

A.1 Field Sampling Selection

All remote sensing studies require the acquisition of appropriate reference data. Lidar metrics were used to pre-stratify the watershed. The LIDAR processing software, Fusion (McGaughey, 2016), was used to create metrics for the watershed at a resolution of 75 feet (approximately 1/8th acre). These metrics describe many attributes of the forest structure. By locating plots across the range of forest structures in the watershed, it is believed that plots will better capture the range of forest types, then if they were randomly located without stratifying. Using a technique based on the literature (Hawbaker, et al., 2009), (Maltamo, Bollandsås, Næsset, Gobakken, & Packalén, 2010), (Gobakken, Korhonen, & Næsset, 2013), and on previous projects for the USDA Forest Service (USFS) and USDI Bureau of Land Management (BLM), the watershed was pre-stratified into bins, and eight to 14 plot locations were randomly chosen for each bin from potential areas of the watershed in that bin. Certain bins made up a higher proportion of the watershed, so these bins were assigned more plots.

2015 parcel data for Pierce County was used to identify the property boundaries and assessed land uses of the properties in the watershed. Parcels without resource land, land use classification were removed. Resource lands are those in the Resource Production and Extraction land use category as defined in WAC 458-53-030 Stratification of assessment rolls—Real property (http://apps.leg.wa.gov/wac/default.aspx?cite=458-53-030).

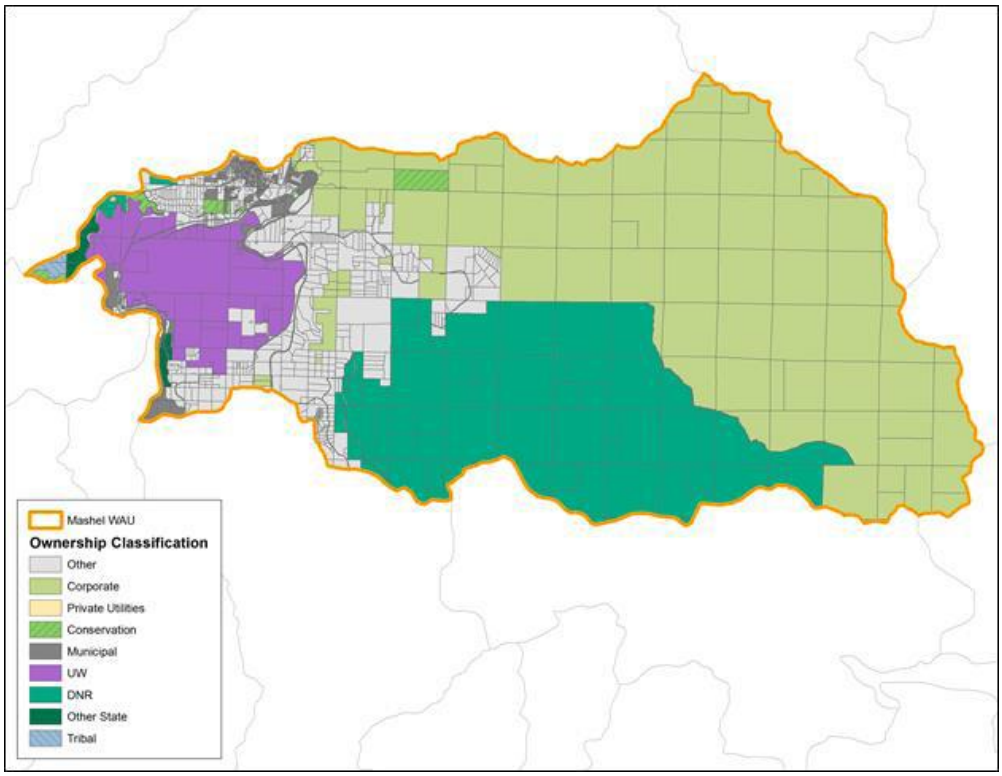

Figure 14*: Land owners of the Mashel watershed*

Figure 15. *An oblique view of an orthomosaic representing the general project area. The yellow line indicates the project boundary, with a perimeter = 84km (52 miles) and area = 230 km^2 (89 square-miles). The snow-capped mountain is Mount Rainier.* Source: Google Earth 2018

Figure 16. *A nadir view of the same orthomosaic, this time showing the project area's riparian composition. 66% of total streams are non-fish type (cyan blue), 21% are fish type (medium blue), and 14% are major rivers considered "shorelines of the state". The project boundary is still indicated by the same yellow line.*

A.2 Stream Buffers

Plots should be located inside of stream buffers. DNR Forest Practices rules and guidelines for stream buffers are complex, and the existing DNR hydrology dataset is known to be inaccurate, particularly in upper reaches. So, following RSAG guidance, stream buffers for the purposes of this project were defined as follows:

- All type F and S streams were buffered 225 feet (three 75ft cells)

- All type N streams were buffered 75 feet (one 75ft cell) for the first 1500 feet upstream from a type F or S stream

All potential field plots located within geographic areas outside of these buffer zones were removed.

Non-Forested areas were removed as well, by looking at two calculated LIDAR metrics, the 80th percentile height and the percent cover. Areas meeting any of the following criteria were removed:

- the metrics could not be calculated
- the 80th percentile height was less than two meters
- the percent cover was less than 10 percent

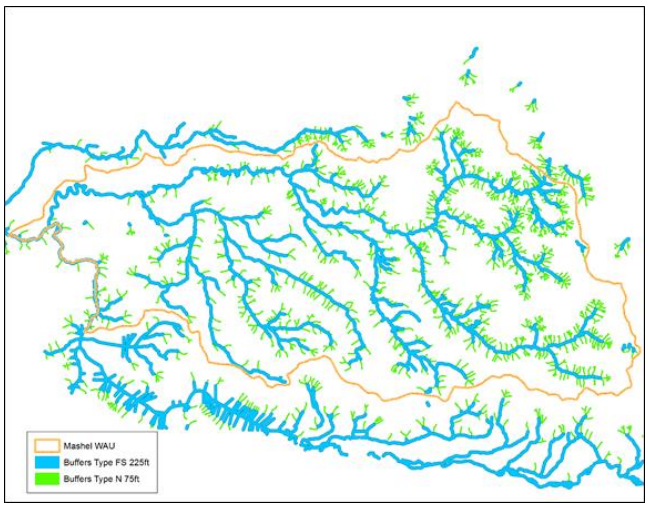

A.3 Principle Component Analysis

LIDAR cells located within these stream buffers were then used in a Principle Component Analysis, which was performed to help narrow down the LIDAR metrics that were used to stratify the landscape. Ten thousand sample points, within stream buffers, were selected randomly and 18 LIDAR metrics were measured at each point. Of these, three metrics explained most of the variability on the landscape. From this, only two were used in defining the final field plots in order to strike a good balance between explanatory ability and the practicality of fieldwork mensuration. Essentially, tree height drives the first principal component, with various metrics having similar importance, while the second principal component is driven by canopy cover.

	Comp.1	Comp.2	Comp.3
1st_cover_above6p5616	0.13	0.41	0.28
all_1st_cover_above6p5616	0.18	0.32	0.32
all_cover_above6p5616	0.13	0.41	0.24
elev_ave_6p5616plus	0.29	-0.01	-0.14
elev_cubic_mean	0.29	-0.08	-0.05
elev_CV_6p5616plus	-0.09	-0.35	0.44
elev_P10_6p5616plus	0.22	0.17	-0.39
elev_P25_6p5616plus	0.26	0.09	-0.29
elev_P50_6p5616plus	0.28	-0.01	-0.13
elev_P75_6p5616plus	0.29	-0.08	-0.03
elev_P80_6p5616plus	0.29	-0.10	-0.01
elev_P95_6p5616plus	0.28	-0.14	0.06
elev_P99_6p5616plus	0.27	-0.14	0.09
elev_quadratic_mean	0.29	-0.05	-0.08
elev_stddev_6p5616plus	0.21	-0.28	0.31
elev_variance_6p5616plus	0.16	-0.27	0.31
FIRST_RETURNS_1st_cover_above6p5616	0.13	0.41	0.28
FIRST_RETURNS_elev_P90_6p5616plus	0.28	-0.12	0.05

Because the metrics chosen are being used to stratify the landscape for field crews, it is helpful to choose metrics that make sense to people at a plot. 80th percentile height is similar to what a field crew would see as plot or stand height. LIDAR measurements of cover are not the same as canopy closure, but low cover occurs in a more open plot, and a high cover occurs in a more closed plot, which a field crew can see. So choosing a height and cover metric to stratify the landscape makes sense from a statistical and practical standpoint.

While several height metrics perform similarly in the first principal component, elev_P80_6p5616plus [the 80th percentile height] was selected. From the second principal component, 1st_cover_above6p5616 [the percent-cover] was selected (*see Figure 10*).

A.4 Defining Plot Bins

The two selected principal component values for the 10k sample points were used to define the bins. The range and distribution of the percent-cover values was used to create four distinct classes.

Within each class the other component, 80th percentile height, subdivided each class into three additional groups. The middle 80th percentile height class is centered on the mean value and is a one standard deviation wide (a ½ standard deviation above and below the mean).

The top height class is everything taller than the middle class, and the bottom height class is everything shorter. The bin definitions are presented below in Figure 11, along with a more ecological interpretation of this bin stratification.

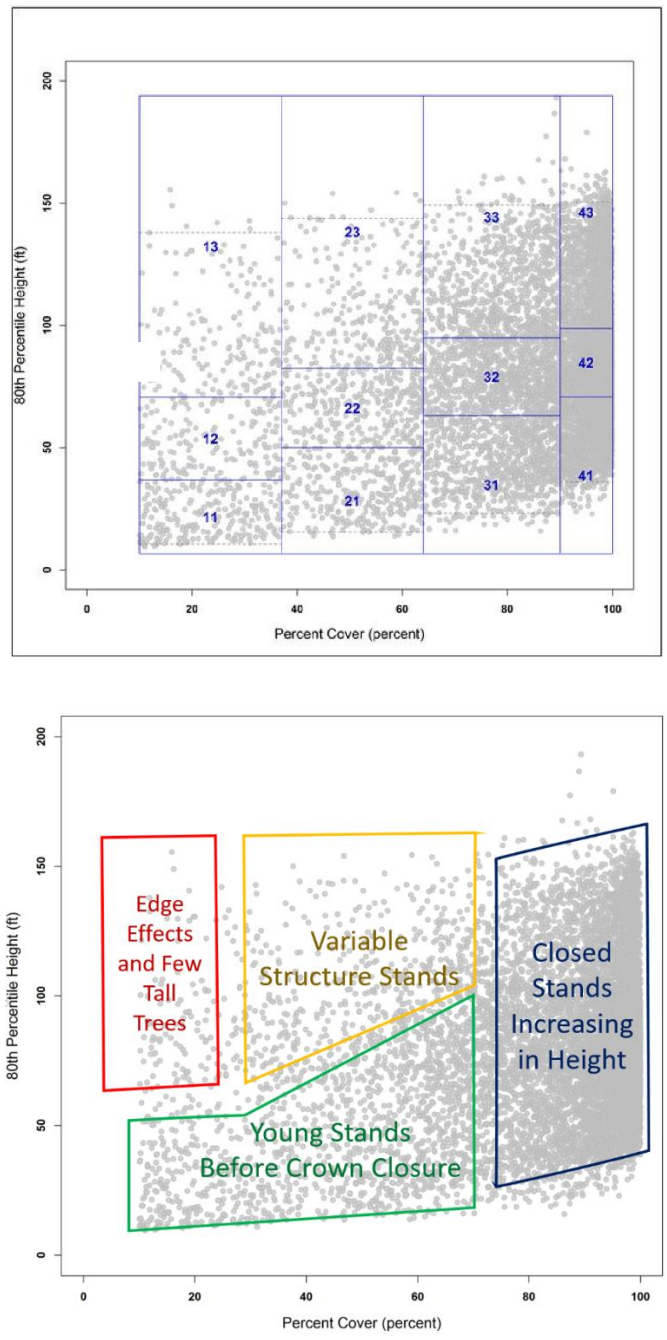

Figure 17. *Plotted results of the principal component analysis. The top image shows the resulting stratification of plot "bins" as outlined by the 12 individual boxes. The bottom image is the same plot but with an ecological interpretation of general forest stands superimposed.*

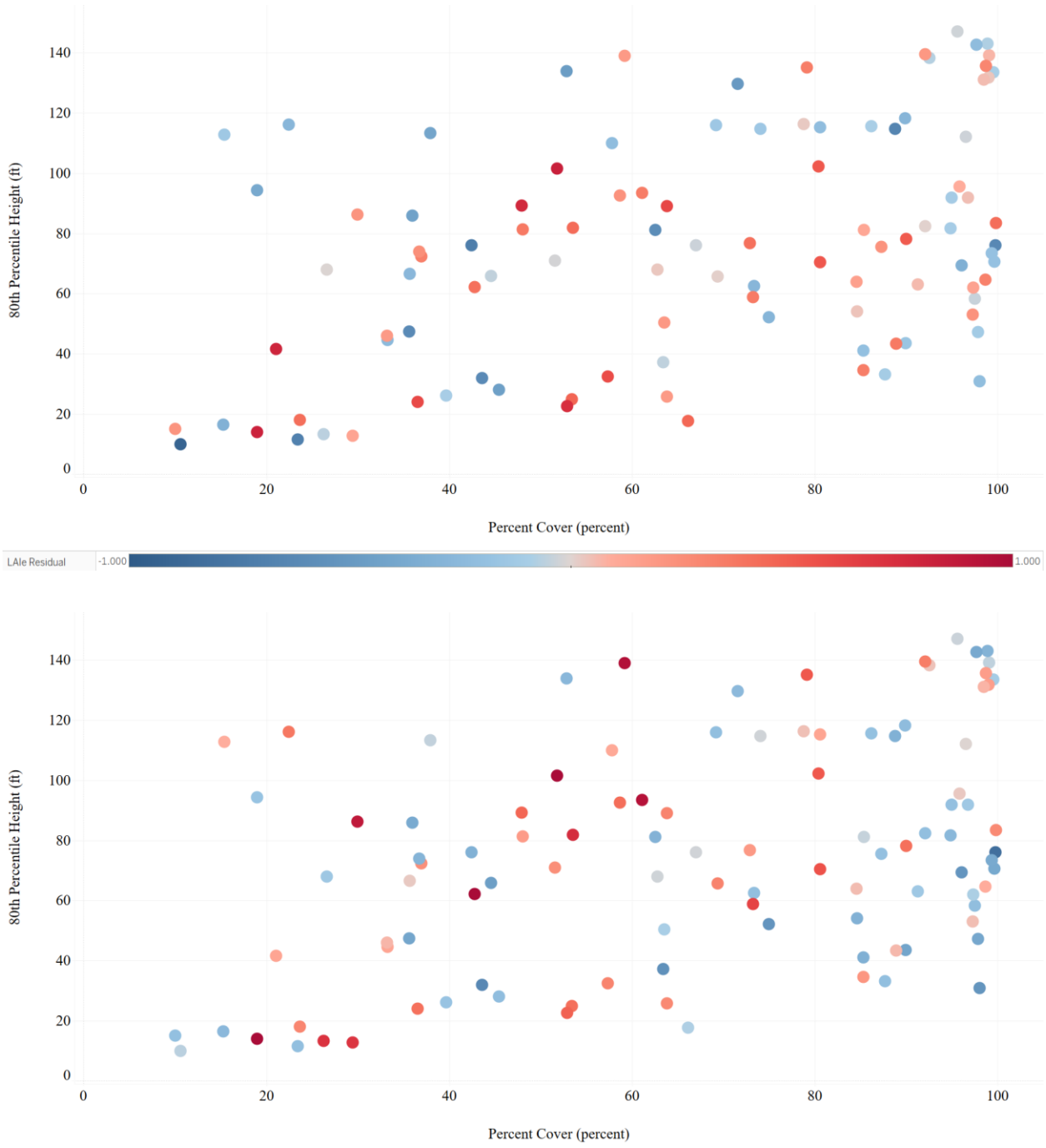

Figure 18. *Plotted results of the principal component analysis for measured field plots. Individual observations are colored based on LAI_E Linear Regression estimate residuals for ALS (top) and SfM (bottom)*

A.5 Fieldwork

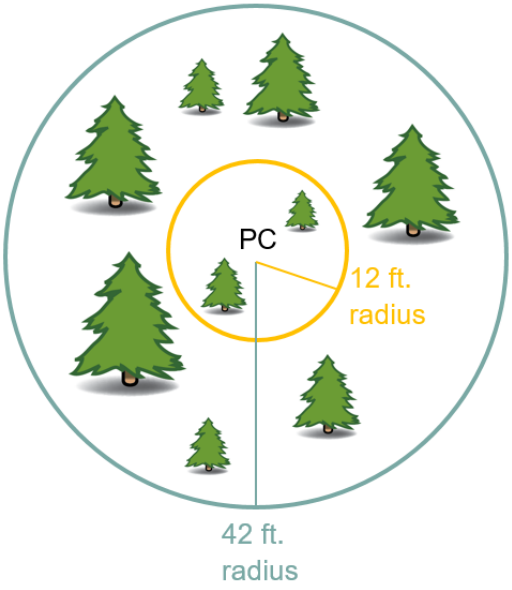

The LIDAR data was flown in 2011 and the plots were measured in 2016, a five-year gap, and the DNR hydrology dataset is known to have inaccurate locations for stream channels. It was therefore very likely that management activity or disturbances could have occurred at plot locations, or that plots were located next to non-existent streams. To prevent wasted time for the field crew, all plots were compared to 2015 imagery, before the field work, to make sure that plots seemed to have the appropriate trees for their bin, and that they were actually in a riparian buffer. Any plots with issues were removed, and the first available alternate plot location was used in its place. After this initial filter mitigation, the final plot locations were randomly selected using bin values. The field crew was tasked with measuring 130 plots total, with 8 to 14 in each bin. 50 extra plots were selected for each bin to account for issues that might arise.

Project details, context, and input/resources from all team members was synthesized to create a field guide detailing the many elements of data collection [supplement: Extensive Riparian Vegetation Monitoring – Field Guide 2016]. This document follows FIA guidelines and was also reviewed by all team members prior to implementation. It contains information explaining both the nuances within the information to be collected and the methodologies and administrative considerations in doing so.

Field Collection efforts transpired 6/1/2016 - 9/17/2016. Two crew members operated throughout the duration of the period, based primarily in University of Washington's Pack Forest, located on the far western section of the Mashel Watershed project area. The graphic above illustrates the layout and dimensions of each field plot. All trees that fell within the large 42.ft radius circle with a DBH >= 5 inches were measured and documented. Trees with DBH < 5 inches were only measured if they fell within the inner 12 ft. radius circle.

A total of 113 plots were sampled. A total of 2,879 trees were sampled, 2,546 of which were alive and 333 dead. Of the living trees, about 90% [2,285] were large trees [DBH greater than 5 in.] and the remaining 264 were small, living trees. Summary metrics by tree species can be found in the next section.

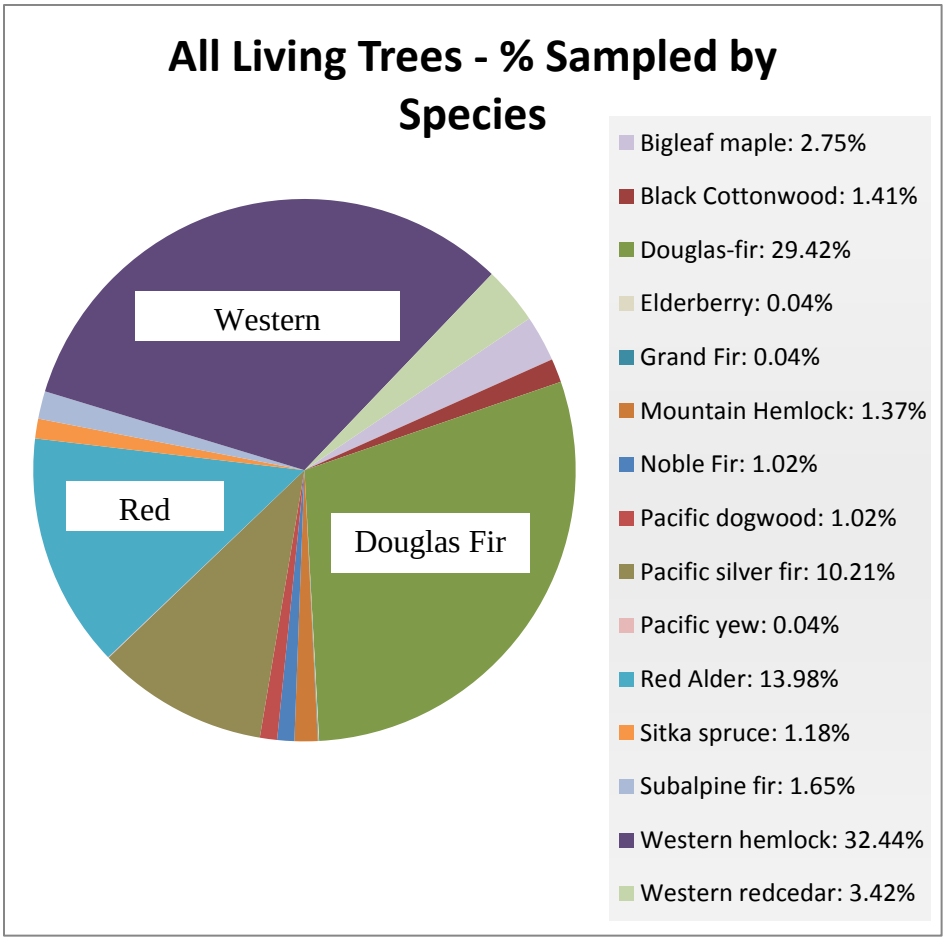

Figure 19 *- A breakdown of tree species composition sampled during field collection 2016.*

A.6 Accuracy and Assumptions of DHP-LAI_E

All point cloud inputs were equal-sized cylinders, clipped with a constant radius of 13m (~42ft.). This was also the plot-radius for field-collected data and aligns among similar best results from previous studies (Richardson, 2010; Riano et al., 2004). While the input for remotely sensed LAI_E is restricted spatially in this way, the digital rendering and subsequent analysis of DHP-LAI_E utilizes of larger visual range of the environment, thus potentially using objects outside the range of 13m in canopy gap fraction calculations. At high LAI_E, small differences in gap fraction can lead to large changes in LAI_E derived from hemispherical photographs.

This limitation can influence DHP-LAI_E accuracy depending on the environmental context of the photo capture. In this study, many outliers in the model estimations seemed to be plots that were located on steeper terrain. To explore this statistically, the lidar linear regression model was chosen and processed through a Oaxaca Decomposition in order to determine if terrain pitch of a plot created bias within LAI_E estimations (Oaxaca 1973). First, all plots are divided into two different groups: those of "more-flat terrain" and those of "more-steep terrain". More-steep terrain is defined as plot center is located on a pitch equal or greater than 30°. Then, each set of data is re-run through the model and the resulting coefficients, variation, and significance is compared in order to determine whether or not a bias exists within the data. The results most likely do not contain enough observations to be statistically significant, but the size and variation of coefficients do suggest that steep terrain may be compromising the derivation process for reference LAI_E and resulting models' estimation of LAI_E.

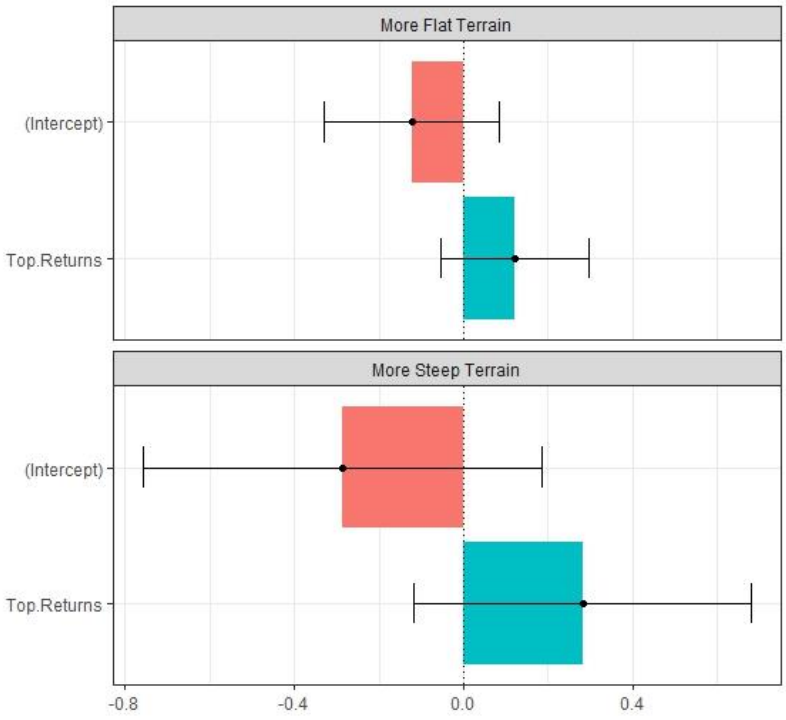

Figure 20. *Output for the Oaxaca Decomposition (two-fold, 95% confidence interval), using the lidar linear regression model. The size of coefficients and variations for plots on more steep terrain is far larger.* (Flat-Terrain N = 77, Steep-Terrain N = 27)

Aside from the difference in visual scope between the terrestrial DHP and aerial platforms, there is also a difference in perspective of these two sensors when viewing the same object. These opposing vantage points means that each will capture elements of the vegetation the other will not. It would be advised, for future remote sensing studies using DHP as reference data, to acquire, process, and analyze multiple photographs per plot in order to increase overall accuracy of LAI_E estimation. Unfortunately, this particular aspect of the accuracy assessment process is very time-consuming, making the prospect of an ongoing program utilizing continuous spatial and temporal coverage of ground-based LAI_E measurements across large landscapes less feasible.

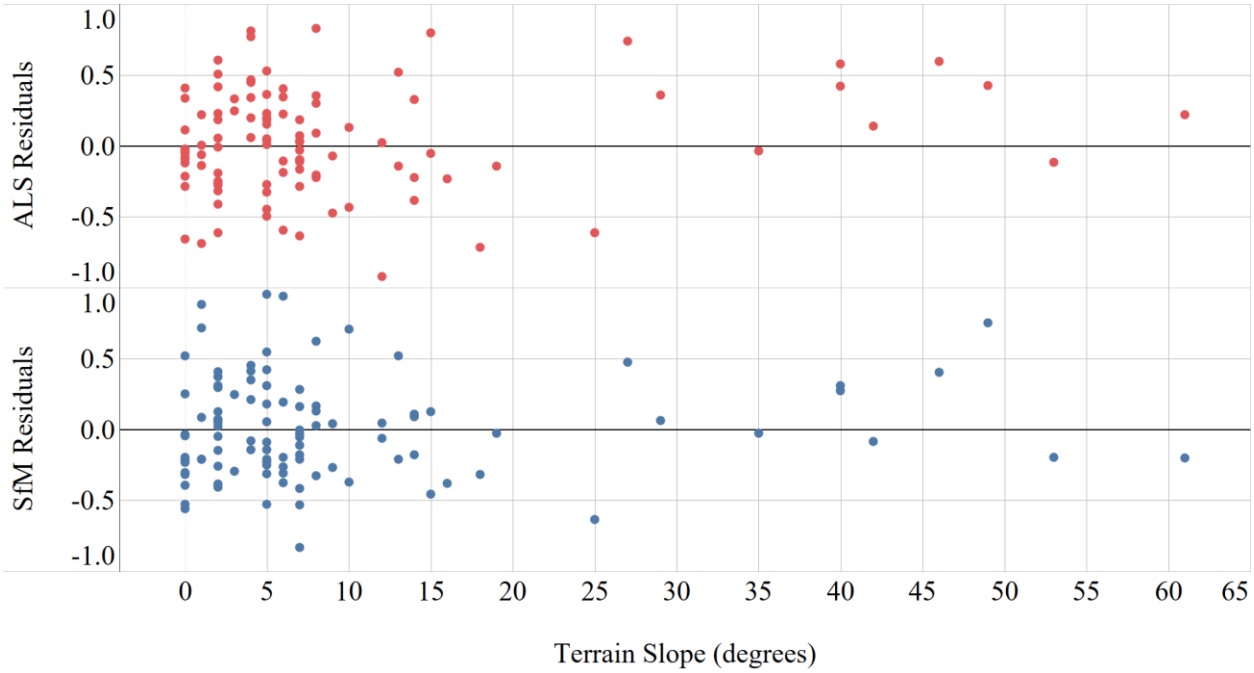

Figure 21. *Linear regression model residuals for both ALS and SfM, plotted against the slope terrain for each respective plot.*

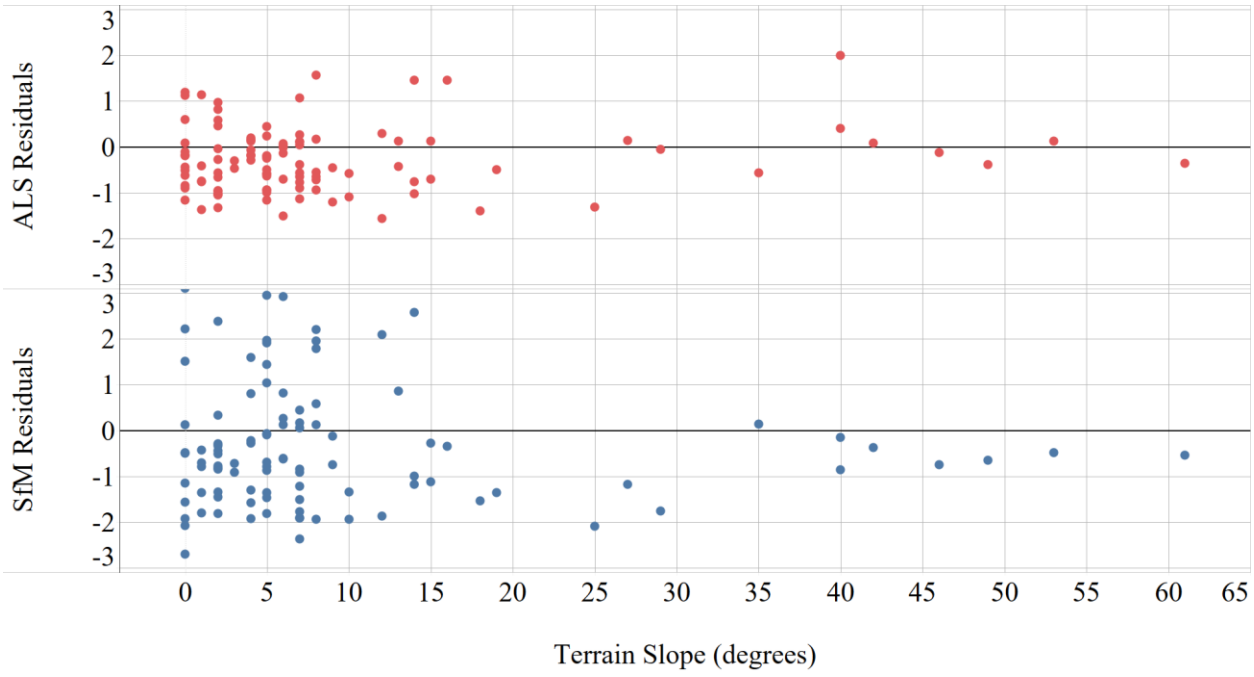

Figure 22. *Beer Lambert Law model residuals for both ALS and SfM, plotted against the slope terrain for each respective plot.*

Appendix B: Digital Hemispherical Photography

The purpose of this supplement is to record the method used in this study for acquiring and analyzing hemispherical photographs. There are many sources of error in this process, and this presents the detailed method used to produce estimates of LAI_E.

B.1 Photograph Acquisition

1. The camera used was Nikon CoolPix 4500 with a Nikon FC-E8 Fisheye lens. This camera was also used in the development of the method for acquiring hemispherical photographs in Zhang et al. (2005). If other cameras are to be used, this guide should be modified.

2. The camera was put into Fisheye mode and manual focus mode.

3. The aperture was set to 5.3

4. The camera was placed on a 1 m tall tripod, brought into an open field and leveled. The shutter speed was then adjusted until the light meter was two "clicks" to the right of the suggested level.

5. The camera was then brought to the plot location, leveled, set to face magnetic north, and set to timer mode.

6. The shutter was depressed and the operator ducked to be out of the field of view of the photograph.

7. If light levels are changing rapidly (as they do at dawn and dusk), the camera should be brought into an open field at regular interviews to adjust the shutter speed using the methodology in step

B.2 Computational Processing

1. Digital Hemispherical Photography (DHP) software was used for the analysis. This software can be obtained for free from Sylvain G. LeBlanc (Sylvain.Leblanc@CCRS.NRCan.gc.ca).

2. Click “Browse Input” and select the image file of the photograph.

3. You will be prompted to select the camera used in obtaining the photograph. If not prompted, select the camera in the drop down menu. If the camera is not shown, consult the software’s user manual.

4. Click “Blue” in Input Options.

5. For the CoolPix 4500, enter 2.2 for Gamma. Consult the software manual if using a different camera.

6. The software breaks the photograph into 10 annulus rings. You can switch between rings using “Up” and “Down”.

7. Make sure “Histogram Logarithm View” is checked

8. Select “Down” until ring 10 is selected.

9. A histogram of the pixel values in the blue band is shown at the right, on a logarithmic scale. The sliders above and below the histogram can be moved to set the thresholds for “foliage” pixels, “mixed” pixels, and “sky” pixels.

10. Each ring will follow a similar pattern in its histogram. There will be a steep peak at the left leveling off to a near linear area, followed by a steep peak at the right.

11. The bottom slider should be set at the left edge of the linear area, at the point where the “slope” of the histogram moves from linear to exponential.

12. The top slider should be set at the right edge of the linear area, at the point where the “slope” of the histogram moves from linear to exponential.

13. If the histogram is not clear, the thresholds can be adjusted using visual inspection of the ring. The area at the left displays the image of the ring. Higher resolution can be achieved using “Full Resolution” and areas denoted as “mixed pixels” will be displayed in green if “Gaps Colour Code” is selected. By moving the sliders, inspecting the histogram, and inspecting the image, the proper threshold can be set.

14. Continue on to each of the next nine rings, following steps 11-13.

15. When finished, LAIE estimates can be retrieved by entering the number of rings the analysis should process in the box “Rings #.” Select “Process” to retrieve the estimates.

16. The upper right window will display the LAIE (displayed as PAIe) at the top column for the rings selected. It will also display the individual LAIE for each of the 10 rings below that.

17. The thresholds for each photo will be saved in a text file and can be accessed at a later date.

18. The output can also be exported to TRACwin. See the user manual for more information.

Appendix C: Point Cloud Specifications

C.1 FUSION Lidar Metric Descriptions

Below is a description of the individual metrics calculated by the Fusion LIDAR processing software for each plot. These are calculated using the CloudMetrics executable. The description is taken from the manual provided with Fusion (McGaughey 2016).

CloudMetrics computes the following statistics using elevation and intensity values for each LIDAR sample:

- Total number of returns
- Count of returns by return number (support for up to 9 discrete returns)
- Minimum
- Maximum
- Mean
- Median (output as 50th percentile)
- Mode
- Standard deviation
- Variance
- Coefficient of variation
- Interquartile distance
- Skewness Kurtosis
- AAD (Average Absolute Deviation)
- MADMedian (Median of the absolute deviations from the overall median)
- MADMode (Median of the absolute deviations from the overall mode)
- L-moments (L1, L2, L3, L4)
- L-moment skewness
- L-moment kurtosis
- Percentile values (1st, 5th, 10th , 20th, 25th, 30th, 40th, 50th, 60th, 70th, 75th, 80th, 90th, 95th, 99th percentiles)
- Canopy relief ratio ((mean - min) / (max – min))

- Generalized means for the 2nd and 3rd power (Elev quadratic mean and Elev cubic mean)

In addition to the above metrics, CloudMetrics also computes various ratios of returns above the specified canopy/ground threshold when the /above:# switch is used:

- Percentage of first returns above a specified height (canopy cover estimate)
- Percentage of first returns above the mean height/elevation
- Percentage of first returns above the mode height/elevation
- Percentage of all returns above a specified height
- Percentage of all returns above the mean height/elevation
- Percentage of all returns above the mode height/elevation
- Number of returns above a specified height / total first returns * 100
- Number of returns above the mean height / total first returns * 100
- Number of returns above the mode height / total first returns * 100

C.2 ALS Point Cloud Processing

Five different threshold variations (0.5m, 1.0m, 2.0m, 5.0m, 10m) were used to render five different Cloudmetrics' outputs, which were then applied to LAI_E models. Of all the variations, the 1-meter threshold produced results with highest overall accuracy. This was reassuring for our reference data too, as 1-meter was the constant height set for the hemispherical field camera. All model results discussed using a lidar point cloud as input are assumed to have been processed using a 1-meter canopy/ground threshold.

C.3 SfM Point Cloud Processing

The SfM point cloud is fundamentally different from the lidar point cloud in that it has far fewer returns that represent ground returns. Because of this, we have to approach the specified canopy/ground threshold elevation much differently. If we continued using the 1-meter threshold, over half (55) of the respective SfM point cloud plots would exhibit zero ground-returns, which would render Beer-Lambert model outputs statistically insignificant and inaccurate. Several variations of thresholds were tested, in order to mimic the behavior of light

attenuation between upper- and full-canopy conditions. These variations were tested following the same process used with lidar data. The most suitable canopy/ground threshold calculated and used in subsequent SfM analyses was a result of breaking all forest-plots into four general groups, based on average stand height, and then assigned four respective thresholds: 3 meters, 7.6 meters, 12.2 meters, and 15.24 meters (10ft., 25ft., 40ft., 50ft.).

Appendix D: Strategy file for Structure-from-Motion Processing

NGATE Default Strategy
-# VERSION is determined by the software. Users should not change the VERSION. For ASM, the version is 2.
VERSION 2
-# NUM_PASSES can be changed. The number of INT_STRAT* and DOUBLE_STRAT* should match the NUM_PASSES.
NUM_PASSES 7
-# KEEP_RSET4 -- keep match results from R Set 4 when the last pass is 1:1. If the last pass is 2:1, ASM always keep results from 4:1. For some posts, the matching at 4:1 may be successful and the matching at 2:1 or 1:1 may fail. In the final DTM, we may or may not keep the results from 4:1. There are pros and cons of keeping results from 4:1. The cons are that those posts may not have high precision. The pros are that those posts may have a more appropriate elevation than interpolated elevation. We suggest that in natural terrain, we should keep results from 4:1. In urban areas, we should not. However, in some cases, this recommendation may not suit your purposes. 1 for YES, and 0 for NO.
KEEP_RSET41
-# RECTIFY_METHOD has three valid values:
-# 0 -- use DTM block center point to shape the transformation and ground to image
-# 1 -- use the center point of left image to shape the transformation
-# 2 -- use the center point of left image to shape the transformation and at
-# the same time, use the Ground to Image to perform the rectification
-# 3 -- use all (0), (1), and (2)
RECTIFY_METHOD0
IMG_REC_TILE_SIZE 48
COMBINE_BANDS 0
MOVING_OBJ_DIM 0
URBAN_CANYON 0
POSITIVE_SLOPE_IN_DEGREE -1
-# FEATHER_BLOCK_EFFECT has two valid values:
-# 0 -- there are not blocking effect in the TSR image generated from the DSM. Therefore, there is no block effect
-# 1 -- there are significant blocking effect in the TSR image due to buildings in an urban area with high resolution frame images.
-# It takes much longer to complete ASM when this is set to 1. However, without this additional process, the DSM could have significant blocking effect and error up to 20 cm from high resolution frame images. This is only available in SOCET GXP 4.1 and later version.
FEATHER_BLOCK_EFFECT 0
IMAGE_STRETCH 0
-# SGM_ALGORITHM:
-# 0 -- not to use SGM smoothness algorithm (because it is slow or in rural area)
-# 1 -- to use a faster version of SGM smoothness algorithm. For high end GPU card, it can speed up.

-# 2 -- to use the original SGM smoothness algorithm. This is the default.
-# 3 -- use local global smoothness constraint.
-# 4 -- use only reliably matched pixels for smoothness constraint.
-# 5 -- original smoothness algorithm with mean and standard deviation to determine similar pixel.This option may be more accurate than option 2.
SGM_ALGORITHM 1
-# OBLIQUE_IMAGES has a default value of 0, indicating that the images are not oblique images.
OBLIQUE_IMAGES 0
-# AMP has a default value of 1, indicating that the ASM will use GPU AMP to speed up. To run ASM with CPU only, set AMP to 2. To run the regular NGATE (without the enhancement, set AMP to 0). To run GPU with NVIDIA CUDA, set AMP to 3. All asm_*_CPU.strategy has AMP set to 2. The only difference between asm_*.strategy and asm_*_CPU.strategy is that this parameter is 1 vs. 2. The regular NGATE portion of image matching does not use GPU card or AMP. AMP stands for Accelerated Massive Parallism. In rural areas, when there is no buildings and houses, the NGATE image matching may be accurate enough and it takes less computing time.
AMP 1
-# USE_MULTIPLE_GPU_CARD. When there are two or more GPU cards and they have similar capacities, using multiple GPU cards can speed up ASM. However, if one GPU card is much more capable than the other GPU card such as a Quadro K5000 card with 1536 CUDA cores and a Quadro 5000 card with 352 CUDA cores, using multiple GPU card may not speed up ASM. When there is only one GPU card, the "Number of Processes" should not exceed 2. When there are two GPU cards with similar capacities, use USE_MULTIPLE_GPU_CARD and the "Number of Processes" can be as large as 4. Unlike NGATE, which uses single thread, ASM uses multi-threading. Even if users want to use CPU only, the "Number if Processes" should be much smaller than for NGATE. Each process for ASM may consume several CPU threads. For example, with a 16 CPU cores computer, the "Number of Processes" should not exceed 4 when using CPU only.
USE_MULTIPLE_GPU_CARD 0
-# SELECT_ONE_STEREO_PAIR_FROM_DIFFERENT_STRIPS has default value of 0: For frame images only, 1 for allowing 1 stereo pair from cross strips. For example, with a "Maximum Number of Image Pairs" = 6, 5 stereo pairs will be selected from the same strip and 1 stereo pair will be from different strips. For instance, two pairs from strip 1, three pairs from strip 2, and one pair from strip 1 and strip 2. There are advantages as well as disadvantages for this option. For repeated patterns on roof tops or even parking strips (these are good image edges), they may be perpendicular or parallel to the epipolar line. When they are parallel to the epipolar line, it is very difficult to match them. However, when there are perpendicular to the epipolar line, we may have a chance to match them. When they are parallel to epipolar line for stereo pairs from the same strip, they should be close to perpendicular to the stereo pairs from different strips. This is the advantage of selecting at least one stereo pair from different strips. However, there are disadvantages as well. Images from different strips may have "moving shadow edges" because different strips may be taken with a significant time difference. For example, image 1 from strip 1 was taken at 10:30 AP while image 2 from strip 2 was taken at 10:45. With a 15 minutes time difference, shadows may have moved. This can cause significant elevation errors.

We have this option for experiment and expert users may try it out. The default value is 0 meaning that we do not allow pairs from different strips.
SELECT_ONE_STEREO_PAIR_FROM_DIFFERENT_STRIPS 0
-# SPIKE_DETECTION_ALGORITHM has three valid options. When users select Maximum Number of Image Pairs to a value > 1 and in urban areas, the SPIKE_DETECTION_ALGORITHM should be 2. This algorithm uses dynamic programming to detect and remove SPIKE and WELL posts. Option 0 uses the NGATE SPIKE detection algorithm, which should NOT be used for ASM. Option 1 uses visibility to help detecting SPIKES.
SPIKE_DETECTION_ALGORITHM 2
-# 3D_POINT_CLOUD_FILTER_TOLERANCE for 3D point cloud generation. The unit is pixel GSD. The default value is 0.5 (or 1/2 of a pixel GSD). In other words, the .75 has the unit of one image GSD. If the image gsd is 20 cm, then, the actual filter tolerance is 0.75 * 0.2 = 0.15 meter or 15 cm. Use a large number for less dense 3D point clouds. Use a smaller number for very dense 3D point clouds.
3D_POINT_CLOUD_FILTER_TOLERANCE 0.75
-# FRAME_IMAGE_EXTREME_LARGE_FORWARD_OVRELAP has a default value of 75 percent. For frame images, when the forward overlap is too large (such as > 75 percent), ASM selects two sets of stereo pairs. One set is stereo pairs of adjacent images from the same strip. The other set is stereo pairs that are not adjacent images, but still from the same strip. This set is good for getting higher DTM precision/accuracy. The combination of the two sets of stereo pairs generate the most accurate and reliable DSM.
FRAME_IMAGE_EXTREME_LARGE_FORWARD_OVRELAP 74
-# The following 20 integers control the aera based image matching algorithms as:
-# 1. Image correlation window size. Must be odd numbers. Suggested values are 7, 9, 11, 13, 15, 17. The speed of NGATE decreases when the window size increases. For flat terrain, the wndow size should be larger than for steep terrain.

-# 2. Edge matching window size in line dimension. Must be odd number.
-# 3. Edge matching window size in sample dimension. Must be odd number. Edge matching is designed to capture elevation discontinuities such as buildings and houses. Because of elevation discontinuities, we should use a smaller window size. On the other hand, too small a window size may produce lots of false matches. The compromise is that the window is not a sqaure. Instead, it is a rectangle. In the line dimension, the size is larger than the size in the sample dimension. The line and smample dimensions are based on the image patches after pairwise rectifications. Suggested values are: 7x5, 9x7, 9x5, 11x7, 11x9, etc. Parameter 2 and 3 are not changed by the software.
-# 4. Image correlation search distance. The search distance should be larger for steep terrain and smaller for flat terrain. The speed of ASM decreases when the search distance increases. The suggested values are from 7 to 19.
-# 5. Edge matching search distance. This number should normally be smaller than the image search distance. It should be larger for steep terrain and smaller for flat terrain. In urban areas, even when the terrain is flat, this number should not be too small in order to match houses and buildings.
-# 6. Minification level of the current pass. Make sure that the specified minification level images are available. Otherwise, ASM bails out.

-# 7. Edge pixel cutoff value. Value greater is considered edge pixel. The default value is 9. If there are too many edge matched points, we should make this number larger. If there are many missing edges, we should lower this number.
-# 8. Positive spike slope limit in degree (0-89)
-# 9. Negative spike slope limit in degree (0-89)
-# 10. Slope limit in degree (0-89) For urban areas with buildings and houses and there are multiple image pairs covering the same area and use multiple imahe pairs per post/point, tje slope limit should be very high (89 degree) in order to have very sharp buidling edges. To allow vertical buildings, set the value to 90. NGATE considers 90 degree as NO high slope detection. The disadvantage is that there may be more blunders.
-# 11. ASM options. 0 -- use both image correlation and edge matching.
-# 1 -- use only image correlation.
-# 2 -- use only edge matching.
-# 3 -- use image correlation and CPU
-# In natural terrain without buildings and houses, option 1 with image correlation only may be good enough because it is faster than option 0. Option 2 is rarely used. It is for research and testing purposes.
-# 12. For NGATE only, smaller window size reduction for image match. This number must be even numbers. The actual window size = parameter_1 - parameter_12. Make sure that the actual window size is at least 5. Suggested values are 0, 2, 4, 6. When the value is 0, it indicates NOT to use a smaller window size for image correlation. The smaller window size is designed to work in urban areas where there are lots of elevation discontinuities such as buildings and houses.
-# 13. Largest Y parallax search distance. When there are Y parallax even after rectification, we set this parameter to > 0. When there is no Y parallax, this parameter should be 0. In most cases even with Y parallax, we may only set its value to be > 0 for the last pass. Suggested values are 1 to 3. If the Y parallex is greater than 3 pixels, you should re-triangulate your images.
-# 14. ASM determines if this is an urban area and need to use a smaller window. If parameter 12 is not zero, this parameter does not matter. It is used only when parameter 12 is 0. 1 for YES and 0 for NO.
-# 15. ASM determines image correlation strategies adaptively. Similar to the Adaptive ATE. But uses a different method (hopefully better method). These parameters are parameter 1 and 4. 1 for YES and 0 for NO.
-# 16. ASM determines parameters 8, 9, and 10 when set to 1. When set to 0, ASM uses parameters of 8, 9, 10 from this file
-# 17. Image buffer size. The suggested values should be: 128, 160, 192, 224, 256, 288, 320. Smaller image buffer size may generate more accurate results at the expense of longer computing. For satellite images or small scale images, the image buffer size can be much larger. The image buffer size has direct impact on the epipolar resampling because ASM uses one set of parameters to perform epipolar resampling for the entire image buffer. This approach is an an approximation and it is dependent on the image buffer size amnong other factors.
-# 18. Cutoff value for isolated edge pixels. In the edge matching window, when the center pixel is an edge pixel, we count the number edge pixels. If precent of the edge pixels is smaller than this number, the edge pixel is considered an isolated edge pixel and we set its value to 0 or non edge pixel. The range is from 50 to 100. The default value is 55.
-# 19. Back match on/off. 1 for on which is the default. 0 for off. In some cases, the back match option may filter out some good points. Turn it off will generate more points. On the other hand,

without back match, the generated DTM may have more blunders. If your DTM does not have blunders, you should turn back match off. If your DTM have many blunders, you should turn back match on.
-# 20. Interpolation method of non-matched point. 0 -- use TIN linear interpolation (default)
-# 1 -- use nearest matched post (for urban areas)
-# 2 -- use GRID linear interpolation
-# Each line has parameters for each pass. Always start from INT_STRAT0 to INT_STRATn where n is the last pass such as 5, 6, 7, etc.

```
-#          1  2  3  4  5  6  7  8  9 10 11 12 13 14 15 16 17 18 19 20
INT_STRAT0 5 7 3 21 15 64 9 90 90 89 1 0 0 0 0 0 224 55 0 0
INT_STRAT1 5 7 3 15 15 32 9 90 90 89 1 0 0 0 0 0 224 55 0 0
INT_STRAT2 5 7 3 15 15 16 9 90 90 89 1 0 0 0 0 0 224 55 0 0
INT_STRAT3 5 7 3 15 15 8 9 90 90 89 1 0 0 0 0 0 224 55 0 0
INT_STRAT4 5 7 3 15 15 4 9 90 90 89 1 0 0 0 0 0 224 55 0 1
INT_STRAT5 5 7 3 21 21 2 9 90 90 89 1 0 0 0 0 0 288 55 0 1
INT_STRAT6 5 7 3 21 21 1 9 90 90 89 1 0 0 0 0 0 352 55 0 0
```

-# The following 15 doubles control the ASM as:
-# 1. Image correlation good neighbor cutoff value.
-# 2. Edge matching good neighbor cutoff value.
-# 3. Image correlation FOM cutoff value.
-# 4. Edge matching FOM cutoff value.
-# 5. Signal power cutoff value. In desert areas, this value should be small from 2 to 8. In other areas, the suggested values are from 3 to 10. If there are still points on water bodies, you need to increase this value. If your image is of high radiometric quality, you can use samller value. If your image is noisy, you should use larger value.

-# 6. Large signal power cutoff value.
-# 7. Image correlation back matching cutoff value.
-# 8. Edge matching back matching cutoff value.
-# 9. X parallax difference cutoff value. Suggested values: 0.5 - 1.0. 1.0 is for extremely steep terrain or urban areas with houses and buildings. It is the ratio of the difference of x parallax vs. the difference of samples. In other words, it is similar to the HIGH_SLOPE detection that uses the slope limit in degree (0-89).
-# 10. Minimum correlation coefficient difference. For noise images or images not well triangulated, we may increase this value at the last two passes. Or if there are blunders, we may increase this value to remove some of the blunders. Suggested values: 0.155 to 0.25
-# 11. Maximum percent edge value difference / 10
-# 12. Signal power difference cutoff value.
-# 13. Second peak difference cutoff.
-# 14. Rough terrain lower FOM cutoff value.
-# 15. Invalid precision distance factor. The default value is 30. To assign more invalid precision 32767 to posts which are not directly measured, you need to decrease this number.

```
-#             1    2    3    4    5    6    7   8   9    10    11   12   13   14   15
DOUBLE_STRAT0 0.1 0.20 0.4 0.80 10.0 54.0 4.1 3.0 1.0 0.180 0.30 9.24 0.10 0.05 30.0
```

DOUBLE_STRAT1 0.1 0.20 0.4 0.80 8.0 54.0 4.1 3.0 1.0 0.180 0.30 9.24 0.10 0.05 30.0
DOUBLE_STRAT2 0.1 0.20 0.4 0.80 6.0 52.0 4.1 3.0 1.0 0.175 0.35 9.24 0.10 0.05 30.0
DOUBLE_STRAT3 0.1 0.20 0.4 0.75 4.0 60.0 4.1 3.0 5.0 0.170 0.40 9.24 0.10 0.05 30.0
DOUBLE_STRAT4 0.1 0.20 0.4 0.75 3.0 68.0 4.1 3.0 10.0 0.165 0.45 9.24 0.10 0.05 30.0
DOUBLE_STRAT5 0.1 0.20 0.4 0.75 2.5 96.0 4.1 3.0 20.0 0.160 0.50 9.24 0.10 0.05 30.0
DOUBLE_STRAT6 0.1 0.20 0.4 0.75 2.0 192.0 4.1 3.0 30.0 0.155 0.55 9.24 0.10 0.05 30.0
-# The following 10 integer parameters are for ASM matching.
-# 1. Support region max search distance for very similar pixels. Very similar pixel is defined by the fourth parameter. Default 25.
-# 2. Similar pixel definition. If two pixels have a intensity value difference of <= 10, it is considered similar pixels. It it scaled to 0-255 range. In other words, if the image has an range of 0 - 511, this value is adjusted by the software by times 2. Default 10
-# 3. Very similar pixel definition. Default 5
-# The first 3 parameters are used to determine "support region" which is very similar to adaptive image matching. Adaptive image matching uses a window size that changes adaptively to the terrain. In flat and/or featureless area, the image window size should increase. In steep terrain, the window size should decrease. The support region is more flexible since it is not a rectangular window anymore. Instead,pixels in the support region are aggregated for matching purpose. To have a larger support region, increase these 4 parameters. To have a smaller support region, decrease these 3 parameters. In natural terrain, decrease these 3 parameters. In urban area with houses and buildings, increase these 3 parameters. In flat area, increase these 3 parameters. In steep area, decrease these 3 parameters. When there are houses with steep rooftops, decrease these 3 parameters.
-# 4. Similar pixel defintion for smoothness constraint. When the difference of image intensity of two pixels are within this number, they are considered similar pixels and a strong smoothness constraint is applied. In urban areas with lots of houses and buildings, increase this number. In natural terrain, decrease this number. This number is image scale independent. Default 10. In other words, it is not dependent on image depth (number of bits).
-# 5. In a support region, when there are this number of pixels that have been matched, it is considered that there are enough reliable matches to determine pixels that are not matched by reion voting. In other words, choose the most frequent macthes in the support region as the "Interpolated match". This is a different way of determining pixels that cannot be matched based on its support region matched pixels. When rooftops are flat, decrease this number. When rooftop are steep, increase this number. Default 20
-# 6. Max number of pixels that a reliable match can be used as smoothness constraint. This is dependent on RSET. At RSET3, this number should be much smaller than at RSET 0. The default for RSET3 is 15. The default for RSET0 is 50. In natural terrain, decrease this number. In urban area with lots of houses and building, increase this number.
-# 7. Threshold value of X parallax difference that is considered an elevation discontinuity. With elevation discontinuity, the smoothness constraint is not applied. This value is depending on RSET level. To enforece more smoothness constraint, increase this number.
-# 8. SGM win size. 0 -- indicates NOT to use SGM logic.
-# 9. Shadow detction. 0 for NO and 1 for YES. For the first few passes, shadow detection logic should be off. In urban areas with shadows such as high resolution frame images, shadow may be a problem. Therefore, set the shadow detection on.

-# 10. Maxinum number of x parallax allowed for the adaptive aggregation algorithm. The value depends on RSET level. The max value must be <= 6 and >= 1
-# 1 2 3 4 5 6 7 8 9 10
SGM_INT_STRAT0 0 0 0 0 0 0 3 0 0 3
SGM_INT_STRAT1 0 0 0 0 0 0 3 0 0 3
SGM_INT_STRAT2 0 0 0 0 0 0 3 0 0 3
SGM_INT_STRAT3 10 25 6 15 30 60 2 3 1 2
SGM_INT_STRAT4 10 25 6 15 30 60 2 3 1 2
SGM_INT_STRAT5 10 25 6 15 30 60 2 3 1 2
SGM_INT_STRAT6 10 25 6 15 30 60 2 5 0 2
-# The following 3 double type parameters are used to control ASM matching.
-# 1. Smoothness constraint small penalty.
-# 2. Smoothness constraint large penalty.
-# 3. percent of pixels in region voting that is greater than this number is considered reliable region voting. In natural terrain, increase this number. In urban areas with flat rooftops, decrease this number. Default is 0.50. It must be within [0.1 and 0.9]
SGM_DOUBLE_STRAT0 0.2 0.3 0.9
SGM_DOUBLE_STRAT1 0.2 0.3 0.9
SGM_DOUBLE_STRAT2 0.2 0.3 0.9
SGM_DOUBLE_STRAT3 0.2 0.3 0.9
SGM_DOUBLE_STRAT4 0.2 0.3 0.9
SGM_DOUBLE_STRAT5 0.2 0.3 0.9
SGM_DOUBLE_STRAT6 0.2 0.3 0.9

Appendix E: Resource Environment Valuation

Existing guides and tools:

- The Measurement of Environmental And Resource Values: Theory and Methods (Freeman et al. 2014)
- Environmental Valuation Reference Inventory (EVRI, http://www.evri.ca)
- Recreation Use Values Database (Oregon State, http://recvaluation.forestry.oregonstate.edu/)
- Ecosystem Services Assessment and Valuation (ARIES N.D, http://aries.integratedmodelling.org//)
- Benefit Transfer Toolkit for Wildlife Recreation, Species, and Habitat (Defenders of Wildlife, Manual)

Appendix F: Benefit Cost Analysis Steps

1. **Specify the set of alternative policies**
    a. A BCA compares the net social benefits of investing one or more alternative policies to the current policy (often referred to as the *status quo* or *counterfactual*).
    b. For many environmental issues these policies can be generally separated from one another by examining their specific answers to two important questions: (1) What amount of damage and costs does the issue impose, especially overtime, and (2) What is it worth to society to implement mitigation and adaptation strategies to avoid or alleviate this potential damage. Naturally-renewable resources that are at risk of exhaustion due to excess use are among the most disputed.
2. **Decide whose benefits and costs have standing**
    a. Whose benefits and costs should be included in the analysis? Some major environmental issues are approached with a global scope, like climate change and ozone depletion. Others remain dependent on the unique set of environmental conditions that benefit and drive local economy.
    b. It's important to consider and evaluate both the individual's perspective (microeconomic), and that of wider, regional-scale regulatory bodies (macroeconomic).
3. **Identify the impact categories, catalog them, and select measurement indicators**
    a. All inputs and outputs that affect those that have standing within the proposed policy. This could be the required resources needed for construction, changes in physical well-being of a population (man or wildlife), new public revenue collected, the increase in value of an ecosystem service, overall impacts, etc.
    b. Is this major impact a benefit or cost? Which populations does it represent or neglect? What is the complexity of uncertainty surrounding it? Is the impact occurring in a primary or secondary market?
4. **Predict the impacts quantitatively over the life of the policy**

a. Many significant ecological processes can occur over long time periods, so environmental BCA's usually apply the rules of dynamic efficiency (change over time) and incorporate the nature of resources being evaluated. Do the resources regenerate? Are they finite? To what extent are future resource supplies affected by today's actions?
b. Efficiency corresponds to maximizing the difference between total benefits and costs; this difference is greatest when marginal benefit equals marginal cost.

5. **Monetize all impacts**
    a. Discern between nominal dollars which occur at a specific time and real dollars, which are adjusted for inflation (also referred to as current dollars and constant dollars, respectively). In BCA, real dollars are always used.
    b. Calculate opportunity costs, especially for any labor that might be involved. Opportunity costs are the value of goods/services that would have been produced had these resources been used instead in the best alternative way.
6. **Discount the benefits and costs to obtain present values**
    a. When considering future benefits and costs to a policy, all values must be converted into their dollar value for today before summing everything together. This allows a common measuring device to evaluate a policy through different points in time.
    b. Money is always worth more to someone today then that same amount in the distant future for four major reasons: inflation, risk, impatience, and/or opportunity cost. So, the analysis must "discount" the costs and benefits expected to occur in the future.
7. **Compute the net present value of each alternative**
    a. Discounting the future, which is the opposite of compounding, converts future dollars to the Present Value (PV). Aggregating the present value for all benefits and costs and then taking the difference will yield the Net Present Value (NPV) for a policy.
    b. A simple rule for BCA is to adopt an alternative if the NPV is positive. When there is more than one alternative to the status quo and all the alternatives are

mutually exclusive, select the policy with the largest NPV. If no NPV is positive, then none of the specified alternatives are superior to the status quo.

8. **Perform a sensitivity analysis [comparing #7 to #4]**
    a. Always test how sensitive the analysis is to initial assumptions. Will changing figures alter the profitability of the policy? One variable worth testing in several iterations is the discount rate, primarily because of its inherent uncertainty.
    b. There is usually a point at which the discount rate can switch the NPV from positive to negative. This is called the switch point. A switch point analysis finds the discount rate which results in NPV = 0. This is also called the Internal Rate of Return [IRR]
        i. Multiple IRRs might exist depending on the function
        ii. IRR is insensitive to the scale of the policy
        iii. Disregarding policy acceptance, the IRR can still always be useful in a sensitivity analysis
9. **Make a recommendation**
    a. The BCA with the highest, positive NPV is generally awarded support. It's important to consider the results of the sensitivity analysis, as even the highest NPV policy may not be the best alternative in all circumstances.
    b. The BCA serves as a recommendation, not a decision. It suggests actions oriented towards a more efficient use of resources. BCA is a useful tool, but often does not have enough clout alone to determine a policy. It should not be considered an authoritative voice in decision making and may not account for important factors of social equity

Appendix G: Remote Sensing of Resource Environment Services

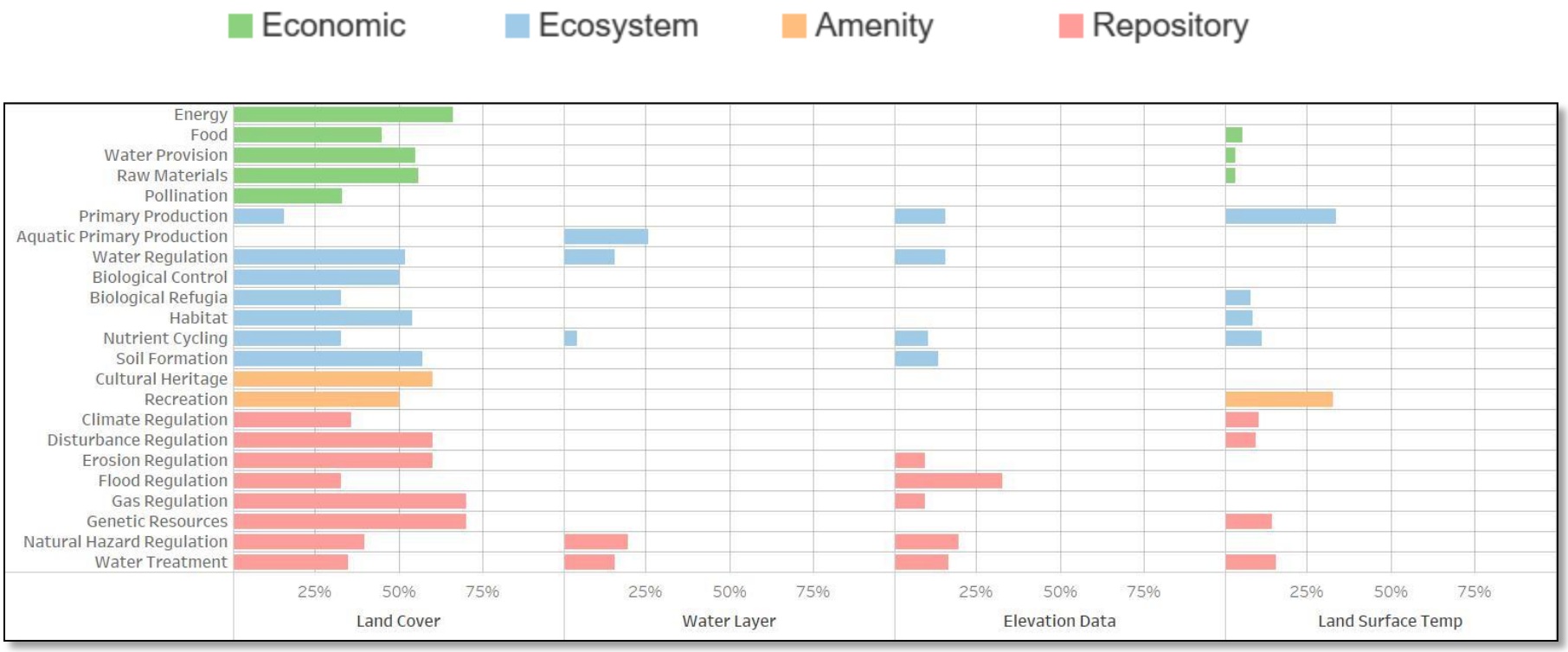

Figure 23. *Percentage of publications that directly utilize remote sensing to assess resource environment services, categorized by respective value-flow. Publications represent 211 distinct studies spanning 1960-2016. Source: adapted from Barbosa et al. (2015), with modifications by the author (Axe, 2018)*

Figure 24. *Percentage of publications that directly utilize remote sensing to assess resource environment services, categorized by respective value-flow. Publications represent 211 distinct studies spanning 1960-2016. Source: adapted from Barbosa et al. (2015), with modifications by Axe (2018).*

Bibliography

Asner, G.P., Scurlock, J.M.O. and A. Hicke, J., 2003. Global synthesis of leaf area index observations: implications for ecological and remote sensing studies, pp. 191-205.

Asner, G.P., Townsend, A.R., Bustamante, M.M.C., Nardoto, G.B., Olander, L.P., 2004. Pasture degradation in central Amazon: linking changes in carbon and nutrient cycling with remote sensing. Global Change Biol. 10, 844-862.

Andersen, Hans-Erik, Robert J. McGaughey, and Stephen E. Reutebuch. 2005. “Estimating Forest Canopy Fuel Parameters Using LIDAR Data.” Remote Sensing of Environment 94 (4): 441–49. doi:10.1016/j.rse.2004.10.013.

Anderson, Martha C. "Simple method for retrieving leaf area index from Landsat using MODIS leaf area index products as reference." Journal of Applied Remote Sensing 6, no. 1 (2012): 063554. doi:10.1117/1.jrs.6.063554.

Archived NAIP Data. (2018). Retrieved from https://www.fsa.usda.gov/programs-and-services/aerial-photography/status-maps/archived-naip-data/index

Babcock, C.R, Finely, A.O., Andersen, H.E., Moskal, L.M., Morton, D.C., Cook, B., Nelson, R., 2017. National-scale aboveground biomass geostatistical mapping with FIA inventory and GLAS data: Preparation for sparsely sampled lidar assisted forest inventory. AGU Fall Meeting Abstracts.

Bagstad, K.J., Villa, F., Batker, D., Harrison-Cox, J., Voigt, B., Johnson, G.W., 2014. From theoretical to actual ecosystem services: mapping beneficiaries and spatial flows in ecosystem service assessments. Ecol. Soc., 19.

Barbier, Edward B. "The Global Greenhouse Effect." *Natural Resources Forum*13, no. 1 (1989): 20-32. doi:10.1111/j.1477-8947.1989.tb00847.x.

Bernknopf, R.L., Brookshire, D.S., McKee, M., and Soller, D.R., 1997, Estimating the societal value of geologic map information—A regulatory application: Journal of Environmental Economics and Management, v. 32, p. 204–218.

Boardman, A. E. (2014). Cost-benefit analysis: Concepts and practice. Harlow, Essex: Pearson.

Brouwer, R., Johnston, R. J., Rolfe, J., & Rosenberger, R. S. (2015). Benefit transfer of environmental and resource values: A guide for researchers and practitioners. Dordrecht: Springer.

Cabello, J., Fernandez, N., Alcaraz-Segura, D., Oyonarte, C., Pineiro, G., Altesor, A., Delibes, M., Paruelo, J.M., 2012. The ecosystem functioning dimension in conservation: insights from remote sensing. Biodivers. Conserv. 21, 3287-3305.

Cai, Y.B, Zhang, H., Pan, W.B., Chen, Y.H., Wang, X.R., 2013. Land use pattern, socioeconomic development, and assessment of their impacts on ecosystem service value: study on natural wetlands distribution area (NWDA) in Fuzhou city, southeastern China. Environ. Monit. Assess. 185, 5111-5123.

Casu, F., M. Manunta, P.s. Agram, and R.e. Crippen. "Big Remotely Sensed Data: Tools, Applications and Experiences." Remote Sensing of Environment 202 (2017): 1-2. doi:10.1016/j.rse.2017.09.013.

Campbell, James B. *Introduction to Remote Sensing*. New York, NY: The Guilford Press, 1996.

Chianucci, F., Disperati, L., Guzzi, D., Bianchini, D., Nardino, V., Lastri, C., . . . Corona, P. (2016). Estimation of canopy attributes in beech forests using true colour digital images from a small fixed-wing UAV. *International Journal of Applied Earth Observation and Geoinformation*,*47*, 60-68. doi:10.1016/j.jag.2015.12.005

Chu, D.A., Kaufman, Y.J., Zibordi, G., Chern, J.D., Mao, J., Li, C.C., Holben, B.N., 2003. Global monitoring of air pollution over land from the Earth Observing SystemTerra Moderate Resolution Imaging Sepctraradiometer (MODIS). J. Geophys. Res.-Atmos., 108.

Coops, N.C.; Hilker, T.; Wulder, M. A.; St-Onge, B.; Newnham, G.; Siggins, A.; Trofymow, J.A. Estimating canopy structure of Douglas-fir forest stands from discrete-return Lidar. Trees-Structure and Function 2007, 21, 295–310.

Dandois, Jonathan P., Marc Olano, and Erle C. Ellis. "Optimal altitude, overlap, and weather conditions for computer vision UAV estimates of forest structure." Remote Sensing 7, no. 10 (2015): 13895-13920.

Doan, H.T.X., Foody, G.M., 2007. Increasing soft classification accuracy through the use of an ensemble of classifiers. Int. J. Remote Sens. 28, 4609-4623.

Eigenbrod, F., Armsworth, P.R., Anderson, B.J., Heinemeyer, A., Gillings, S., Roy, D.B., Thomas, C.D., Gaston, K.J., 2010. The impact of proxy-based methods on mapping the distribution of ecosystem services. J. Appl. Ecol. 47, 377-385.

Evans, Jeffrey S., Andrew T. Hudak, Russ Faux, and Alistair M. S. Smith. 2009. "Discrete Return Lidar in Natural Resources: Recommendations for Project Planning, Data Processing, and Deliverables." Remote Sensing 1 (4): 776–94. doi:10.3390/rs1040776.

Evans, T.P., Kelley, H., 2008. Assessing the transition from deforestation to forest regrowth with an agent-based model of land cover change for south-central Indiana (USA). Geoforum 39, 819-832.

Everitt, Brian. 1998. "The Cambridge Dictionary of Statistics." Cambridge, UK New York: Cambridge University Press. ISBN 0521593468.

Frank, S., Fuerst, C., Koschek, L., Makeschin, F., 2012. A contribution towards a transfer of the ecosystem service concept to landscape planning using landscape metrics. Ecol. Indic. 21, 30-38.

Fonstad, Mark A., James T. Dietrich, Brittany C. Courville, Jennifer L. Jensen, and Patrice E. Carbonneau. "Topographic structure from motion: a new development in photogrammetric measurement." Earth Surface Processes and Landforms 38, no. 4 (2013): 421-430.

Freeman, A. M., Herriges, J. A., & Kling, C. L. (2014). *The measurement of environmental and resource values: Theory and methods*. New York: RFF Press.

Fuller, D.O., 1998. Trends in NDVI time series and their relation to rangeland and crop production in Senegal, 1897-1993. Int. J. Remote Sens. 19, 2013-2018.

Gong, Peng, Ruiliang Pu, and John R. Miller. "Correlating Leaf Area Index of Ponderosa Pine with Hyperspectral CASI Data." *Canadian Journal of Remote Sensing*18, no. 4 (1992): 275-82. doi:10.1080/07038992.1992.10855332.

Gower, S.t., Kucharik, C.J., Norman, J.M., 1999. Direct and indirect estimation of leaf area index, fAPAR, and net primary production of terrestrial ecosystems. Remote Sensing of Environment 70 (1), 29-51.

Halabisky, M., Moskal, L.M., Hall, S.A., 2011. Object-based classification of semi-arid wetlands. Journal of Applied Remote Sensing 5 (1), 053511.

Hoa, F., Zhang, X., Ouyang, W., Skidmore, A.K., Toxopeus, A.G., 2012. Vegetation NDVI linked to temperature and precipitation in the upper catchments of yellow river. Environ. Model. Assess. 17, 389-398.

Haralick, R., Shanmugam, K., and Dinstein, I. (1973), Textural features for image processing. *IEEE Trans. Syst. Man Cybern.* SMC-3(6):610-621

Helm, Dieter. *Economic Policy towards the Environment*. Oxford, UK: Blackwell, 1996.

Jennings, S. "Assessing forest canopies and understorey illumination: canopy closure, canopy cover and other measures." Forestry 72, no. 1 (1999): 59-74. Accessed June 21, 2017. doi:10.1093/forestry/72.1.59.

Kastens, J.H., Kastens, T.L., Kastens, D.L.A., Price, K.P., Martinko, E.A., Lee, R.Y., 2005. Image masking for crop yield forecasting using AVHRR NDVI time series imagery. Remote Sens. Environ. 99, 341-356.

Kennedy, Robert E., Philip A. Townsend, John E. Gross, Warren B. Cohen, Paul Bolstad, Y.q. Wang, and Phyllis Adams. "Remote Sensing Change Detection Tools for Natural Resource Managers: Understanding Concepts and Tradeoffs in the Design of Landscape Monitoring Projects." *Remote Sensing of Environment*113, no. 7 (2009): 1382-396. doi:10.1016/j.rse.2008.07.018.

Keohane, Nathaniel O., and Sheila M. Olmstead. *Markets and the Environment*. Washington, DC: Island Press, 2016.

Kross, A., Seaquist, J.W., Roulet, N.T., Fernandes, R., Sonnentag, O., 2013. Estimating carbon dioxide exchange rates at contrasting northern peatlands using MODIS satellite data. Remote Sens. Environ. 137, 234-243.

Leblanc, S.G., Chen, J.M., Fernandes, R., Deering, D.W. and Conley, A., 2005. Methodology comparison for canopy structure parameters extraction from digital hemispherical photography in boreal forests. Agricultural and Forest Meteorology, 129(3-4): 187-207.

Leblanc, S.G., 2006. Digital Hemispherical Photography Manual. Natural Resources

Canada, Canada Centre for Remote Sensing.

Lim, K., Treitz, P., Baldwin, K., Morrison, I., Green, J., 2003. Lidar remote sensing of biophysical properties of tolerant northern hardwood forests. Canadian Journal of Remote Sensing 29 (5), 658-678.

Littell, Jeremy S.; Peterson, David L.; Riley, Karin L.; Liu, Yongquiang; Luce, Charlie H. 2016. A review of the relationships between drought and forest fire in the United States. Global Change Biology. doi: 10.1111/gcb.13275.

Linard, C., Tatem, A.J., Gilbert, M., 2013. Modelling spatial patterns of urban growth in Africa. Appl. Geogr. 44, 23-32.

Liu, J., Li, Y., Liu, S.B., 2013. Prediction models of soil organic matter based on spectral curve in the upstream of Heihe basin. Spectrosc. Spectr. Anal. 33, 3354-3358.

Lüdeke, M., Janecek, A., Kohlmaier, G.H., 1991. Modelling the seasonal CO_2 uptake by land vegetation using the global vegetation index. Tellus 43B, 188-196.

Mathews, Adam, and Jennifer Jensen. "Visualizing and Quantifying Vineyard Canopy LAI Using an Unmanned Aerial Vehicle (UAV) Collected High Density Structure from Motion Point Cloud." *Remote Sensing*5, no. 5 (2013): 2164-183. doi:10.3390/rs5052164.

McGaughey, R. J. 2016. FUSION/LDV: Software for LIDAR Data Analysis and Visualization. Seattle, WA: United States Department of Agriculture Forest Service Pacific Northwest Research Station. Retrieved from http://forsys.cfr.washington.edu/fusion.html

Millennium Ecosystem Assessment (Program). (2005). Ecosystems and human well-being. Washington, D.C: Island Press.

Mkhabela, M.S., Bullock, P., Raj, S., Wang, S., Yang, Y., 2011. Crop yield forecasting on the Canadian Prairies using MODIS NDVI data. Agric. Forest Meteorol. 151, 385-393.

Morsdorf, F., Ko¨ tz, B., Meier, E., Itten, K.I., Allgo¨wer, B., 2006. Estimation of LAI and fractional cover from small footprint airborne laser scanning data based on gap fraction. Remote Sensing of Environment 104 (1), 50–61.

Monsi, M., Saeki, T., 2005. On the factor light in plant communities and its importance for matter production. Annals of Botany 95, 549-567.

Moskal, L.M, Dunbar, M.D, Jakubauskas, M.E., 2004. Visualizing the forest: a forest inventory characterization in the Yellowstone National Park based on geostatistical models. Message from the Tatras: Geographical Information Systems & Remote Sensing in Mountain Environmental Research. 219-232.

Moskal, L. M. and A. Cooke, 2015. Feasibility of applying remote sensing to a riparian stand conditions assessment, Agreement No. IAA 15-118 (Revised 1/1/2015); Prepared for Washington Department of Natural Resources.

Mozumbder, C., Reddy, K.V., Pratap, D., 2013. Air pollution modeling from remotely sensed data using regression techniques. J. Ind. Soc. Remote Sens. 41, 269-277.

Muraoka, H., Koizumi, H., 2009. Satellite ecology (SATECO)-linking ecology, remote sensing and micrometeorology, from plot to regional scale, for the study of ecosystem structure and function. J. Plant Res. 122, 3-20.. Modeling multiple ecosystem services, biodiversity conservation, commodity production, and tradeoff at landscape scales. Front. Ecol. Environ. 7, 4-11.

Nelson, E., Mendoza, G., Regetz, J., Poloasky, S., Tallis, H., Cameron, D.R, Chan, K.M.A., Daily, G.C., Goldstein, J., Kareiva, P.M., Londdorf, E., Naidoo, R., Ricketts, T.H., Shaw, M.R., 2009

Numata, I., Soares, J.v., Roberts, D.A., Leonidas, F.C., Chadwick, O.A., Batista, G.T., 2003. Relationships among soil fertility dynamics and remotely sensed measures across pasture chronosequences in Rondonia, Brazil. Remote Sens. Environ. 87, 446-455.

Oaxaca, R. (1973). Male-female wage differentials in urban labor markets. International Economics Review, 14(3), 693–709

Palacios-Orueta, a., Huesca, M., Whiting, M.L., Litago, J., Khanna, S., Garcia, M., Ustin, S.L, 2012. Derivation of phenological metrics by function fitting to time-series of spectral shape indexes AS1 and AS2: Mapping cotton phenological stages using MODIS time series. Remote Sens. Environ. 126, 148-159.

"People and Pixels." 1998. doi:10.17226/5963.

Pierce, L.L. and Running, S.W., 1988. Rapid Estimation of Coniferous Forest Leaf Area Index Using a Portable Integrating Radiometer. Ecology, 69(6): 1762-176

Portney, Paul and John Weyant. 1999. *Discounting and Intergenerational Equity*, Resrouces for the Future, Washington, D.C.

Potter, C., Gross, P., Klooster, S., Fladeland, M., Genovese, V., 2008. Storage of carbon in US forests predicted from satellite data, ecosystem modeling, and inventory summaries. Slim. Change 90, 269-282.

Prabakaran, C., Singh, C.P., Panigraphy, S., Parihar, J.S., 2013. Retrieval of forest phenological parameters from remote sensing-based NDVI time-series data. Curr. Sci. 105, 795-802.

Pralle, Sarah B., 2006. *Branching Out, Digging In: Environmental Advocacy and Agenda Setting*. Washington: Georgetown University Press

Riano, D., Valladares, F., Condes, S., Chuvieco, E., 2004. Estimation of leaf area index and covered ground from airborne laser scanner (Lidar) in two contrasting forests. Agricultural and Forest Meteorology 124 (3-4), 269-275.

Reyers, B., O'Farrell, P.J., Cowling, R.M., Egoh, B.N., Le Maitre, D.C., Vlok, J.H.J, 2009. Ecosystem services, land-cover change, and stakeholders: finding a sustainable foothold for a semiarid biodiversity hotspot. Ecol. Soc., 14.

Richardson, Jeffrey J., L. Monika Moskal, and Soo-Hyung Kim. "Modeling approaches to estimate effective leaf area index from aerial discrete-return LIDAR." Agricultural and Forest Meteorology 149, no. 6-7 (2009): 1152-160. doi:10.1016/j.agrformet.2009.02.007.

Richardson, Jeffrey J, and L. Monika Moskal. 2011. "Strengths and Limitations of Assessing Forest Density and Spatial Configuration with Aerial Lidar." Remote Sensing of Environment 115 (10): 2640–51. doi:10.1016/j.rse.2011.05.020.

Rindfuss, Ronald R., Stephen J. Walsh, B. L. Turner, Emilio F. Moran, and Barbara Entwisle. "Linking Pixels and People." Land Change Science Remote Sensing and Digital Image Processing, 2012, 379-94. doi:10.1007/978-1-4020-2562-4_22.

Roots, O.O., Roose, A., Eerme, K., 2011. Remote sensing of climate change, long-term monitoring of air pollution and stone material corrosion in Estonia. Int. J. Remote Sens. 32, 9691-9705.

Rosentreter, Roger, Richard H. Waring, and William H. Schlesinger. "Forest Ecosystems, Concepts, and Management." *Journal of Range Management* 39, no. 5 (1986): 480. doi:10.2307/3899464.

Rouse, J.W, Haas, R.H., Scheel, J.A., and Deering, D.W. (1974) 'Monitoring Vegetation Systems in the Great Plains with ERTS.' *Proceedings, 3rd Earth Resource Technology Satellite (ERTS) Symposium*, vol. 1, p. 48-62.

Running, S., and Coughlan, J. (1988), A general model of forest ecosystem processes for regional applications: I. Hydrologic balance, canopy gas exchange, and primary production processes. Ecol. Mod. 42:125–154

Schwind, Michael. "Comparing Lidar and Photogrammetric Point Clouds - 19/01/2018." GIM International. January 19, 2018. Accessed February 18, 2018. https://www.gim-international.com/content/article/comparing-Lidar-and-photogrammetric-point-clouds.

Snavely, Noah, Steven M. Seitz, and Richard Szeliski. "Modeling the World from Internet Photo Collections." *International Journal of Computer Vision*80, no. 2 (2007): 189-210. doi:10.1007/s11263-007-0107-3.

Solberg, S., Næsset, E., Hanssen, K.H., Christiansen, E., 2006. Mapping defoliation during a severe insect attack on Scots pine using airborne laser scanning. Remote Sensing of Environment 102 (3-4), 364-376.

Spillman, C.M, Imberger, J., Hamilton, D.P., Hispey, M.R., Romero, J.R., 2007. Modelling th effects of Po River discharge, internal nutrient cycling and hydrodynamics on biogeochemistry of the Northern Adriatic Sea. J. Mar. Syst. 68, 167-200

Sturck, J., Poortinga, A., Verburg, P.H., 2014. Mapping ecosystem services: the supply and demand of flood regulation services in Europe. Ecol. Indic. 38, 198-211.

Thomas, S.C. and Winner, W.E., 2000. Leaf area index of an old-growth Douglas-fir forest estimated from direct structural measurements in the canopy. Canadian Journal of Forest Research-Revue Canadienne De Recherche Forestiere, 30(12): 19221930.

Urban, Daniel, Kaiyu Guan, and Meha Jain. "Estimating Sowing Dates from Satellite Data over the U.S. Midwest: A Comparison of Multiple Sensors and Metrics." Remote Sensing of Environment 211 (2018): 400-12. doi:10.1016/j.rse.2018.03.039.

Van Zyl, Hugo. (2014). The Economic Value and Contribution of the Simon's Town Penguin Colony, Cape Town, South Africa. 10.13140/RG.2.2.11103.46244.

Vaughn, N.R., Moskal, L.M, Turnblom, E.C., 2012. Tree species accuracies using discrete point lidar and airborne waveform lidar. Remote Sensing 4(2), 377-403.

Vose, J.M., Sullivan, N.H., Clinton, B.D. and Bolstad, P.V., 1995. Vertical Leaf-Area Distribution, Light Transmittance, and Application of the Beer-Lambert Law in 4 Mature Hardwood Stands in the Southern Appalachians. Canadian Journal of Forest Research-Revue Canadienne De Recherche Forestiere, 25(6): 1036-1043.

Wang, Jun. 2013. "People, Institutions, and Pixels: linking remote sensing and social science to understand social adaptation to environmental change". University of Michigan doctoral dissertation.

Wardlow, B.D., Egbert, S.L, 2008. Large-area crop mapping using time-series MODIS 250m NDVI data: an assessment for the US Central Great Plains. Remote Sens. Environ. 112, 1096-1116.

Waring, R.H.; Pitman, G.B. Modifying lodgepole pine stand of change susceptibility to mountain pine-beetle attack. Ecology 1985, 66, 889–897. [Google Scholar]

Wallace, K.J., 2007. Classification of ecosystem services: problems and solutions. Biol. Conserv. 139, 235-246

Wallace, Luke, Arko Lucieer, Zbyněk Malenovský, Darren Turner, and Petr Vopěnka. "Assessment of Forest Structure Using Two UAV Techniques: A Comparison of Airborne Laser Scanning and Structure from Motion (SfM) Point Clouds." *Forests*7, no. 12 (2016): 62. doi:10.3390/f7030062.

Westoby, M.J., J. Brasington, N.F. Glasser, M.J. Hambery, and J.M. Reynolds. "'Structure-from Motion' photogrammetry: A low-cost, effective tool for geoscience applications." *Geomorphology* 179 (2012): 300-314.

Wulder, M. A., S. E. Franklin, and M. B. Lavigne. "High Spatial Resolution Optical Image Texture for Improved Estimation of Forest Stand Leaf Area Index." *Canadian Journal of Remote Sensing*22, no. 4 (December 1, 1996): 441-49. doi:10.1080/07038992.1996.10874668.

Wulder, Mike A., Ellsworth F. Ledrew, Steven E. Franklin, and Mike B. Lavigne. "Aerial Image Texture Information in the Estimation of Northern Deciduous and Mixed Wood Forest Leaf Area Index (LAI)." Remote Sensing of Environment 64, no. 1 (1998): 64-76. doi:10.1016/s0034-4257(97)00169-7.

Zheng, Guang; Moskal, L. Monika. 2009. "Retrieving Leaf Area Index (LAI) Using Remote Sensing: Theories, Methods and Sensors." Sensors 9, no. 4: 2719-2745.

Zinnert, J.C., Shiflett, S.A., Vick, J.K., Young, D.R., 2011. Woody vegetative cover dynamics in response to recent climate change on an Atlantic coast barrier island: a remote sensing approach. Geocarto Int. 26, 595-612.